ADVANCED QUANTUM TECHNOLOGIES
www.advquantumtech.com

Manipulating Single-Photon Emission from Point Defects in Diamond and Silicon Carbide

*Marianne Etzelmüller Bathen * and Lasse Vines*

Point defects in semiconductors are emerging as an important contender platform for quantum technology (QT) applications, showing potential for quantum computing, communication, and sensing. Indeed, point defects have been employed as nuclear spins for nanoscale sensing and memory in quantum registers, localized electron spins for quantum bits, and emitters of single photons in quantum communication and cryptography. However, to utilize point defects in semiconductors as single-photon sources for QT, control over the influence of the surrounding environment on the emission process must be first established. Recent works have revealed strong manipulation of emission energies and intensities via coupling of point defect wavefunctions to external factors such as electric fields, strain and photonic devices. This review presents the state-of-the-art on manipulation, tuning, and control of single-photon emission from point defects focusing on two leading semiconductor materials—diamond and silicon carbide.

1. Introduction

Point defects in semiconductors are versatile systems that can trap charge carriers in highly localized quantum states. Depending on the semiconductor band gap and spin-orbit coupling strength, certain point defects may exhibit millisecond spin coherence times, room temperature (RT) spin manipulation and bright single-photon emission at RT.[1] Effectively, point defects combine all the necessary ingredients for facilitating quantum computers and networks: i) qubits based on either photon polarization or electron spin,[2] ii) gate operations can be applied to isolated spin systems,[3] and iii) single-photon emission is available for read-out and secure information transfer over large distances and within quantum computer systems.[4]

To employ point defects for nanoscale sensing,[5] as spin center qubits for quantum information processing[6] and single-photon emitters (SPEs) for quantum communication,[4] several requirements must be met. In the case of sensing, there is some flexibility, as both the point defect spin and light emission are potential degrees of freedom to be manipulated and detected. Quantum communication networks and information processors, on the other hand, set stricter conditions.[7,8] Although we will briefly touch upon the point defect spin degree of freedom, we will herein mainly focus on manipulation and control of the single-photon emission process.

Single-photon emitters are enticing quantum objects with application areas including cluster-state quantum computing,[9] quantum key distribution (QKD),[10,11] and quantum repeaters.[12] The requirements for functionalizing point defects as quantum light sources include bright emission, low multi-photon emission probability and negligible spectral diffusion for the emitted objects. In other words, brightness, purity, and indistinguishability of the single-photon emission must be established (see, e.g., refs. [4, 13] for a summary of the concrete metrics). Emission brightness translates into a high single-photon emission or collection rate, with required efficiencies in excess of 50% or 90–99% for quantum key distribution and optical quantum computing, respectively. In many cases, coupling to waveguides and cavities will be necessary to reach such a goal.[14] High single-photon emission purity is characterized by a low multi-photon emission probability, that is, a low value for the second-order correlation function $g^{(2)}(\tau)$ at zero delay time. Extreme photon purities are likely required in optical quantum repeaters and computers, in excess of 99.9% ($g^{(2)}(0) < 0.001$), while QKD is more lenient. Photon indistinguishability is verified in the Hong-Ou-Mandel two-photon interference experiment, where identical photons always exit the beam splitter together with a 50:50 rate.[15] In sum, to employ point defect SPEs for the production of many-photon entangled states for, for example, quantum repeaters and linear optical quantum computation, the key metrics for emission efficiency, purity and indistinguishability are likely restricted to errors well below ~1%.[4] InGaAs quantum dots is an example system offering SPE purity and indistinguishability above 99%, albeit at a lower brightness at ~15% efficiency.[16] The

Dr. M. E. Bathen, Prof. L. Vines
Department of Physics/ Centre for Materials Science and Nanotechnology
University of Oslo
Oslo N-0316, Norway
E-mail: bathen@aps.ee.ethz.ch
Dr. M. E. Bathen
Advanced Power Semiconductor Laboratory
ETH Zürich
Physikstrasse 3, Zürich 8092, Switzerland

The ORCID identification number(s) for the author(s) of this article can be found under https://doi.org/10.1002/qute.202100003

DOI: 10.1002/qute.202100003

combination of high photon extraction efficiency (85%), entanglement fidelity (88%) and indistinguishability (90%) was more recently demonstrated.[17] Comparably, ref. [18] showed QD emission with a 57% extraction probability and indistinguishability of 97.5%. Point defect emitters have yet to reach this level of purity and indistinguishability.

The most studied quantum color center (in bulk semiconductors) is the nitrogen-vacancy (NV) center in diamond, consisting of a substitutional nitrogen atom next to a carbon vacancy.[19,20] The NV center is a room-temperature single-photon emitter[21] exhibiting millisecond spin coherence times,[22] and has (among other notable advances) been successfully employed for nanoscale biomedical imaging.[23,24] However, diamond suffers from challenges in large-scale wafer manufacturing, and fabrication of nanophotonics devices for SPE integration is difficult to scale. More recently, other materials have emerged as strong contenders, including silicon and silicon carbide (SiC),[1,25] both having wafer-based and mature fabrication readily available.

Semiconductor color centers are sensitive to changes in their surroundings. Indeed, the local environment provides multiple pathways toward decoherence and inhomogeneous emission energies, in addition to opportunities for control over the defect emission and quantum state. Strong coupling to strain and charge fluctuations in the surrounding environment are important sources for spectral diffusion of point defect emitters, and strategies for enhancing the spectral stability include employing defects with inversion symmetry,[26] applying external electromagnetic fields[27] and attaining local environment control.[28] Indeed, indistinguishable photons have been obtained from, for example, silicon-vacancy (SiV) centers in diamond[26] and the Si vacancy (V_{Si}) in 4H-SiC.[27] However, such achievements require that the defect emitter is first identified, the full emission spectrum should be known, and manipulation protocols must be established. These topics have been intensively investigated over recent years and constitute the motivation for the present report.

In this progress report, we provide a status update on the recent advances in manipulating single-photon emission from point defects in semiconductors, with a particular emphasis on how to manipulate defect emission after the luminescent center has been identified. Single-photon emitters have been detected in a broad range of semiconductor material systems, but only a handful have been assigned to a specific defect center—including, for example, the SiV, NV and germanium-vacancy (GeV) centers in diamond, and the V_{Si}, divacancy, nitrogen-vacancy and carbon antisite-vacancy pair defects in silicon carbide. Herein, we will focus on materials encompassing defects that have been identified as viable quantum contenders, namely diamond and silicon carbide, and discuss recent theoretical and experimental progress on controlling the defect charge-state and emission. In this context, mapping the vibronic fine structure and response of an SPE to external perturbation such as strain and electromagnetic fields will be discussed. SiC and diamond constitute the main focus, but we will briefly mention the presence of SPEs in other materials as well. The report is not intended as an exhaustive review, and the reader is therefore directed to other reports for further information on, for example, various solid-state single-photon sources,[4,29] spin-based quantum technologies in semiconductors,[2,30] novel color centers[31,32] and

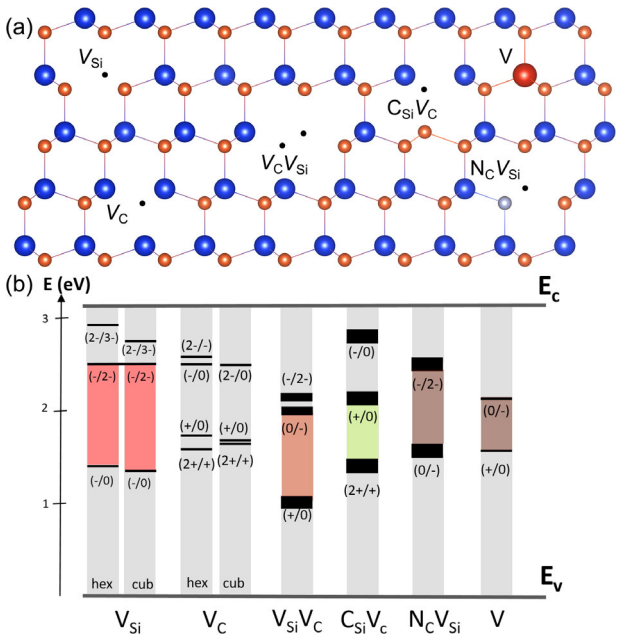

Figure 1. Point defects in 4H-SiC. a) Schematic of various point defects in the 4H-SiC lattice (Si atoms in blue, C atoms are orange, missing atoms denoted by black dot), including the Si vacancy (V_{Si}), C vacancy (V_C), divacancy ($V_{Si}V_C$ or VV), carbon antisite-vacancy pair ($C_{Si}V_C$ or CAV), nitrogen-vacancy center (N_CV_{Si} or NV) and vanadium impurity (V). b) Energy levels in the 4H-SiC band gap for the V_{Si}, V_C, VV, CAV, NV, and V defects. The quantum compatible charge state for each defect type is highlighted by the colored regions.

SPE material platforms,[33] SiC for quantum applications,[34,35] diamond[36–38] and SiC[14] nanophotonics, and density functional theory (DFT) calculations to study point defects for quantum technology (QT).[39,40]

The report is organized as follows. First, in Section 2, a brief introduction to point defects in semiconductors as quantum contenders will be provided, followed by a summary of the most relevant host materials to be discussed herein in Section 3. Thereafter, we turn to the main topics of the present report: charge-state control and device integration are covered in Section 4, and emission tuning in Section 5. In Section 6, we briefly summarize some recent progress on coupling point defect emitters to photonic devices, while future perspectives and conclusions are provided in Sections 7 and 8, respectively.

2. Point Defects as Quantum Contenders

A point defect in a semiconductor lattice, either in the form of a vacancy, interstitial or substitutional defect, may introduce energy levels within the semiconductor band gap. These energy levels represent charge-state transitions, where the defect may capture holes or electrons from the valence or conduction bands, respectively. Example point defects are shown for the case of 4H-SiC in **Figure 1**a, including the Si vacancy (V_{Si}),[41,42] C vacancy (V_C),[43] divacancy ($V_{Si}V_C$ or VV),[44] C antisite-vacancy pair ($C_{Si}V_C$ or CAV),[45] nitrogen-vacancy center (N_CV_{Si} or NV)[46] and vanadium impurity (V).[47,48]

Defects with shallow energy levels, that is, levels close to the band edges, are termed dopants and are often intentionally

introduced to enhance the material's conductivity. Dopants may be potential quantum contenders, both alone (e.g., phosphorous in silicon[25]) and in combination with intrinsic defects (e.g., the NV centers in diamond[20] and SiC[49]). However, most isolated dopants fall outside the scope of the present Progress Report due to their lack of single-photon emission properties. Deep-level defects, on the other hand, exhibit charge-state transition levels far from the band edges and can act as carrier traps and recombination centers.[1] Intriguingly, certain deep-level defects are promising qubit hosts, as the deep energy levels give rise to highly localized electron (or hole) states with minimal interference from the surrounding environment. In other words, the localized orbitals that arise from disturbing the crystalline lattice can enable trapping of charge carriers having long spin coherence times and exhibiting single-photon emission characteristics.

The two main features of point defects in semiconductors that mark them as viable quantum contenders are coherent spin manipulation and single-photon emission. The spin state in question may be that of either the nucleus (of native or impurity type) or a charge carrier (hereafter referred to as an electron) trapped at a defect in a certain charge state.[2] Emission from point defects may arise from excitations to a different charge state or to an internal excited state.[50] Single-photon emission events from point defects usually involve the latter excitation type, while optically detected charge-state transitions typically result in broad emission lineshapes. Internal excitations are often accompanied by a sharp zero-phonon line (ZPL) and individual photons being emitted at definite time intervals. Importantly, QT compatible properties commonly manifest in only one of each defect's charge states. For instance, the colored regions in Figure 1b highlight the bright and spin-active charge states of the relevant quantum centers in 4H-SiC. Note that the carbon vacancy (V_C) in 4H-SiC is not a quantum contender,[51] as opposed to its Si vacancy counterpart.[1,52]

Of course, point defects in semiconductors are not the only available quantum platform. Qubit operation has been demonstrated using properties such as electronic and nuclear spin, charge and photon polarization. Popular implementations of these degrees of freedom include superconducting Cooper pairs, trapped ions/atoms and quantum dots (see, e.g., refs. [4, 29] for an overview). Quantum dots (QDs), particularly of the self-assembled kind, do possess color center and SPE capabilities,[13,53] but the process of self-assembly is accompanied by a certain randomness in the QD shape and size distribution. Accordingly, an ensemble of quantum dots may emit at a broad range of different energies and intensities,[4] with Fourier-limited linewidths being reported for emission from single QDs.[54,55] Point defects in semiconductors, on the other hand, often exist in a more homogeneous environment. Although local environmental variations do exist also in epitaxially grown material, point defect emission is largely reproducible. For instance, ref. [28] recently showed that depleting the charge environment surrounding divacancies ($V_{Si}V_C$) in 4H-SiC reduced emission linewidths down to 20 MHz, which is close to the Fourier lifetime limit of ~11 MHz.[56] Herein, we elucidate how we can exploit the reliable fabrication and emission properties of bulk semiconductors to control, manipulate and shift single-photon emission originating from semiconductor point defects.

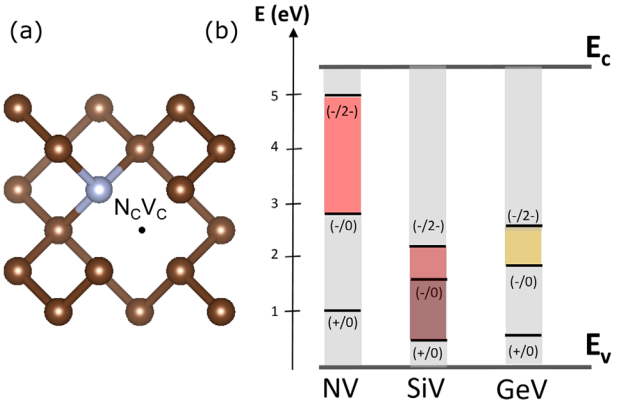

Figure 2. Point defects in diamond. a) Schematic of a nitrogen-vacancy (NV) defect in the diamond lattice (N atom gray, C in brown). b) Energy levels in the diamond band gap for the NV, Si-vacancy and Ge-vacancy defects. The quantum compatible charge state for each defect type is highlighted by the colored regions.

3. Quantum Compatible Point Defects and Their Host Materials

Spurred by the success of diamond and SiC, single-photon emitters have been detected in several different semiconductor materials. Important material characteristics for hosting long spin coherence times and single-photon emission include a wide band gap, low spin-orbit coupling and the existence of spinless nuclear isotopes.[1] The spin state of deep-level defects may be employed for, for example, quantum logic operations, memory and sensing, with the emitted single photons providing complex spin-photon interfaces and a potential for reliable spin-photon entanglement. Although quantum spintronics with point defects is outside the scope of the present progress report, we will here include a brief glimpse into the rich world of spin-based QT. The reader is directed to, for example, refs. [2, 30] for further details.

Note that quantum defects are commonly formed by particle irradiation and hence randomly scattered over some distribution. Recent alternatives to form point defects in a more deterministic manner include proton beam writing[57] and femtosecond laser writing.[58,59]

3.1. Diamond

Among the various solid-state qubit and SPE contenders, the NV center in diamond (**Figure 2**a) is almost certainly the most studied and explored for QT. The nitrogen-vacancy complex in its negative charge state (NV^-) is a $S = 1$ spin center[60] and room-temperature single-photon emitter,[20] with a ZPL wavelength of 637 nm.[61] Charge-state transitions of the NV center and the stability range of the bright negative state are illustrated in Figure 2b. Over the years, the electronic structure of the NV center has become well understood,[19,62,63] and recent theoretical advances include detailed calculations of the luminescence lineshape[64,65] and the effect of environmental coupling on NV^- emission.[66] The luminescence from NV^- encompasses a sharp zero-phonon line (ZPL) and a broad phonon side-band (PSB), resulting in a Debye–Waller factor (DWF) of only ~3–5%, necessitating

waveguide integration or coupling to cavities for reliable utilization of single photons emitted from the diamond color center.

The localized electron spin trapped at NV^- can be coherently controlled, with RT spin coherence times reaching ~2 ms in ^{12}C-enriched nanodiamonds.[22] Comparing to the microsecond coherence times of superconducting qubits, NV^- center spins are highly stable and even suitable for quantum memory applications. However, the ZPL emission wavelength is not optimal for integration with fiber optic technology, and therefore less attractive for, for example, spin-photon entanglement due to photon loss over distance, making the NV center perhaps most promising for its capabilities as a highly responsive quantum sensor with nanoscale resolution. Indeed, NV^- center spins in diamond are sensitive to minute magnetic field variations and can facilitate nanoscale magnetometers[67,68] and imaging at ambient conditions.[23] An important property of diamond (and SiC) in this context is that the material is non-toxic and biocompatible, allowing NV centers to be employed for nanoscale imaging of biological tissue. Additionally, both the spin and luminescence signals of point defects are sensitive to temperature,[69,70] and the sensitivity of the localized NV^- center spin to temperature facilitates optically detected nanoscale thermometry.[71,72]

Despite the NV center hitherto receiving the most attention, other defect complexes in diamond have been demonstrated to possess comparable, if not superior, properties. Indeed, both the silicon-vacancy (SiV) and germanium-vacancy (GeV) complexes exhibit inversion symmetry, which mark them as highly robust toward spectral diffusion caused by stray electric fields and local strain variations.[33] The negatively charged SiV complex (SiV^-) in diamond is a $S = 1/2$ center with a near-infrared (NIR) ZPL at 738 nm,[73] and can boast of a high Debye–Waller factor of 70%[21] compared to the NV center. Moreover, coherent localized spin control has been demonstrated for both NV^- and SiV^-,[74] while indistinguishable photons have been obtained in the case of SiV.[26] However, SiV^- spin coherence times are as low as ~40 ns at 4 K[75] with 10 ms spin lifetimes being attainable only at 100 mK,[76] representing a significant obstacle toward scalable operation. Interestingly, the imbalanced SiV^- electronic spin ($S = 1/2$) makes the center sensitive to a phonon-mediated dynamic Jahn-Teller relaxation, causing limited electron spin coherence times.[77] An alternative strategy is utilizing the neutral and spin-balanced SiV^0, for which longer spin coherence times approaching 1 s, a >90% Debye-Waller factor[78] and coherent spin manipulation[79] were recently demonstrated. The GeV complex has comparable properties to SiV, including inversion symmetry and ~70% of the emission being channeled into the ZPL at 602 nm.[80] Additionally, GeV shares the non-ideal thermal trend of SiV spin lifetimes with spin coherence times in the ~100 ns range at 5 K.[81] In fact, several of the group-IV color centers in diamond exhibit single-photon emitter characteristics,[82] including, for example, the tin-vacancy (SnV) defect with a zero-phonon line at 619 nm and a Debye–Waller factor of ~41%.[83]

3.2. Silicon Carbide

Silicon carbide (SiC) is an emerging quantum platform that benefits from mature fabrication on the wafer-scale. SiC exists in a plethora of different polytypes, with 3C, 4H and 6H being the most prominent configurations, and where several of the polytypes have been demonstrated to host SPEs.[1,34,84,85] The different polytypes exhibit slightly different emitter characteristics and therefore provide an opportunity to select the desired emission properties based on the wide variety of defects and lattice configurations that are available. While 3C has a cubic structure, 4H is hexagonal and contains both hexagonal (h) and pseudo-cubic (k) lattice sites. Similarly, the hexagonal 6H polytype accommodates three orientations labeled h, k_1 and k_2. SiC has a wide band gap (2.3 eV for 3C, 3.0 eV for 6H and 3.26 eV for 4H-SiC) and low spin-orbit coupling, marking it as a suitable quantum material platform.[1,86]

Among the most studied emitters in SiC we find the carbon antisite-vacancy pair (CAV or $C_{Si}V_C$) emitting in the red, the silicon vacancy (V_{Si}) emitting in the near-infrared (NIR), and the divacancy (VV or $V_{Si}V_C$) and the nitrogen-vacancy center (NV or N_CV_{Si}) that both emit at near-telecom wavelengths. See the illustration in Figure 1a for example defect configurations. Importantly, the CAV, V_{Si}, VV and NV defects in SiC have all been identified as room-temperature single-photon emitters with coherent spin control being demonstrated.[52,87–90]

The ultrabright AB-lines, appearing in photoluminescence spectra of (mostly) p-type 4H-SiC at ~640–680 nm, arise from the positively charged $C_{Si}V_C$ with a $S = 1/2$ ground state spin and occurring in the hh, kk, hk, and kh configurations.[87,91]

The V1, V1′, and V2 zero-phonon lines in 4H-SiC, with corresponding wavelengths of 861, 858, and 916 nm, have been attributed to the negatively charged Si vacancy.[52,92–94] Recently, V1 and V2 were assigned to V_{Si}^- at h and k lattice sites, respectively, with V1′ stemming from a higher-lying excited state of $V_{Si}^-(h)$ compared to that of V1.[95,96] The characteristic zero-phonon lines related to V_{Si}^-, V1 and V1′, are shown in **Figure 3**a. The corresponding excitation for $V_{Si}^-(k)$, V2′, has been theorized[97,98] but not detected. Similar identification is available for V_{Si} in 6H-SiC,[99] based on density functional theory calculations utilizing the Δ-self consistent field (Δ-SCF) method.[64] Importantly, V_{Si}^- has a DW factor of 8–9%,[88,97,100] which is higher than that of NV^- in diamond. The V_{Si}^- spins organize in a $S = 3/2$ configuration,[94,101] and single-photon emission (Figure 3b) and coherent spin control (Figure 3c) can both be detected at room temperature.[52] Millisecond spin coherence times are attainable, but in that case cryogenic temperatures (~10 K) are required. Additionally, the localized spins at V_{Si} in 4H- and 6H-SiC facilitate optically detected nanoscale thermometry[102,103] and magnetometry,[104,105] and the V_{Si} has a favorable interface for spin-photon entanglement that might facilitate cluster-state quantum computing.[106–108] However, the V_{Si} is metastable with respect to transformation into the CAV in p-type 4H-SiC material,[41,45,87,109] with the transformation barrier depending on the Fermi level in the sample.[110] Therefore, V_{Si} is mostly studied in n-type or intrinsic 4H (and 6H) SiC.

The neutrally charged divacancy (VV^0) in 4H-SiC is a highly stable room-temperature SPE with $S = 1$, >1 ms spin coherence times[111] and giving rise to at least four ZPLs named PL1-PL4.[84,88] They arise at 1.1–1.2 eV in 4H-SiC, are assigned to the four different combinations of h and k lattice sites, and exhibit DW factors of around 6–7%.[56,96,99,112] The near-telecom emission wavelengths provide a favorable spin-photon interface for VV^0 in 3C and 4H SiC with regard to maintaining

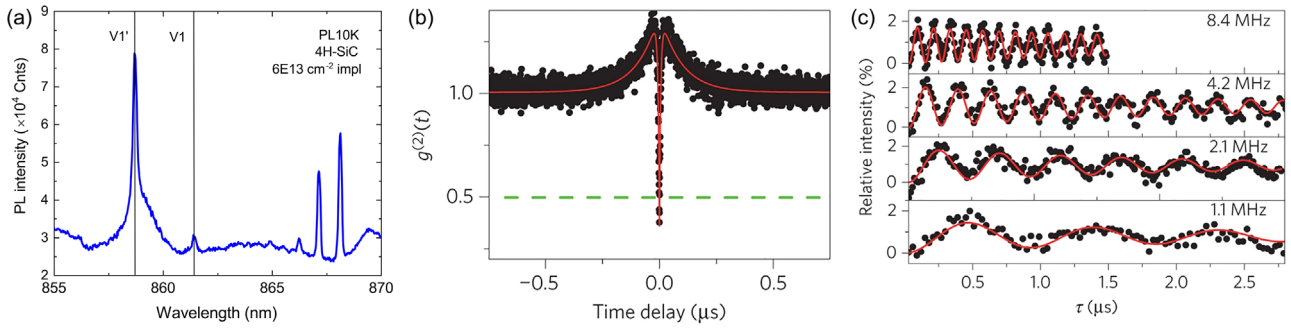

Figure 3. Quantum characteristics of the Si vacancy in 4H-SiC. a) Representative PL spectrum highlighting the sharp zero-phonon lines (ZPLs) originating from the negatively charged Si vacancy (V_{Si}^-) at a hexagonal (*h*) lattice site in 4H-SiC: V1′ and V1. The corresponding ZPL from $V_{Si}^-(k)$, V2, appears at 916 nm and is not shown. b) Autocorrelation measurement for a single V_{Si} center in 4H-SiC. c) Room-temperature coherent spin manipulation of a single V_{Si} center in 4H-SiC. Panels (b) and (c) are reproduced (adapted) with permission.[52] Copyright 2015, Springer Nature.

entanglement over large distances.[56] The favorable magneto-optical properties,[112] spin dynamics,[113–115] and pathways for decoherence[116] of VV centers have been studied extensively, and a recent work proposed universal coherence protection for VV spins by hybridizing an applied microwave drive.[117] Intriguingly, divacancy defects are also suitable for high-precision magnetometry, and have even been successfully entangled with nuclear spins in SiC.[118,119]

Similar to VV, the NV center ($N_C V_{Si}$) has been shown to be a promising qubit candidate and single-photon emitter in several SiC polytypes.[46,49,120,121] The NV center emits at telecom wavelengths, in a similar range to that of the divacancy, which would ease integration with optic fiber technologies as compared to, for example, NV^- in diamond. Recently, coherent manipulation of single NV center spins in 4H-SiC was demonstrated,[89] paving the way toward future utilization of NV centers in SiC for QT.

Transition metal impurities are currently being investigated as potential luminescent spin centers in (particularly) 4H and 6H SiC, but these efforts are still in the early stages. Identification is underway, but accomplishing controlled manipulation of single-photon emission will likely require additional efforts. For that reason, transition metal impurities fall outside the scope of the present work. Examples of potential candidates include vanadium (indicated in Figure 1),[48,122,123] chromium,[124,125] molybdenum,[123,126] complexes between the carbon vacancy (V_C) and niobium,[127] tungsten,[128] and titanium.[129]

3.3. Other Materials

Single-photon emission has been observed to originate from several other semiconductor materials, however, most of the emitters have not been identified, or identification is still at an early stage. Therefore, detailed understanding of spin- and emission-related fine-structure, and advanced manipulation protocols, have yet to be implemented. Below, we summarize recent progress in some promising materials for the future.

Silicon immediately arises as a potential candidate, considering the streamlined material and device fabrication processes that are already available. Indeed, phosphorous impurities at a Si lattice site can store a quantum state for over 30 s,[25] facilitating their use in a potential Kane quantum computer.[33] However, the P impurities lack single-photon source capabilities, and will therefore not be considered herein. Recently, however, color centers in Si were found to emit single photons at telecom wavelengths, where the G center arising from the carbon-interstitial carbon-substitutional complex was identified as a prominent SPE candidate.[130,131] Manipulation of single-photon emission to obtain indistinguishable photons, achieve emission-based quantum sensing and tune emission energies may potentially result from further investigations.

Two-dimensional materials are also of interest for SPE operation and as a quantum platform,[132] where, for example, hexagonal boron nitride (*h*-BN) existing in single- or multilayer structures has become the subject of growing attention. Importantly, a broad range of bright and stable room-temperature single-photon emitters have been detected,[133–135] marking *h*-BN as an exciting and versatile quantum platform. However, even though both calculations[136–138] and detailed experiments[139,140] have been performed in order to identify the color centers responsible for the bright emission from 2D *h*-BN, secure identification is still lacking.

Where SPEs in *h*-BN have been attributed to point defects introducing levels within the wide band gap (~6 eV), quantum emission from 2D transition metal dichalcogenides (TMDCs)[141,142] is ascribed to localized, weakly bound excitons.[4,132] Unfortunately, single-photon emission in TMDCs is restricted to cryogenic temperatures, while *h*-BN, SiC and diamond facilitate RT operation of defect SPEs. Nonetheless, quantum emitters in, for example, WSe_2 exhibit fascinating properties, such as Zeeman splitting[141] and engineering of emitter arrays via strain fields.[143] At the time of writing, there was no report on single-photon indistinguishability for emission from *h*-BN and TMDC materials, which restricts their application potential in advanced quantum technology schemes.

Color centers that emit individual photons have been detected in various other wide-band gap semiconductor materials, including ZnO, ZnS, GaN, and AlN,[33] but material-related challenges complicate defect utilization for QT. Emission lineshapes from ZnO and ZnS, for instance, are broad due to large phonon involvement. The nitrides (e.g., GaN and AlN), on the other hand, are more inclined to exhibiting narrow emission lines. For instance, room-temperature single-photon emission was demonstrated for both GaN[144,145] and wurtzite AlN films,[146] and

tentatively assigned to nitrogen vacancy and divacancy complexes in the latter case. However, defect levels in AlN tend to occur too close to the band edges to facilitate single-photon emission.[33,147,148] Possible solutions have been proposed, including alloying AlN with transition metals[147] and application of strain to the nitrogen vacancy.[148]

Notably, excitonic involvement is often found in the case of single-photon emission. For instance, both interlayer or indirect[149] and defect-bound[150] exciton-related single-photon emission have been demonstrated. The former exciton type refers to the case where the electron and hole are spatially located in different layers, and is often studied in van der Waals structures such as TMDC bilayers. Furthermore, a recently collected ODMR (optically detected magnetic resonance) signal was attributed to bound exciton states at the SiV^0 center in diamond.[79]

4. Charge-State Control and Electronic Device Integration

Identifying the defects responsible for quantum effects such as single-photon emission and spin manipulation is crucial for utilizing point defects in quantum computing, communication and sensing devices. Once identification is in place, control over the defect formation process, thermal response and, particularly, charge state should be established. In this section, we highlight important progress in functionalizing point defects for quantum applications by means of electric field application and integration with electronic devices. Electrical control over the quantum state constitutes a considerable advantage for current superconductor-based electronic qubits, and will likely ease the combination of conventional computer technology with novel quantum platforms.

As discussed above, point defects may exist in several different charge states depending on the semiconductor's Fermi level. However, in most cases, only one of the charge states (e.g., singly negative for NV in diamond and V_{Si} in SiC) is quantum compatible and showcasing features such as single-photon emission and spin manipulation. This issue is illustrated by the shaded regions in Figures 1b and 2b, which show that the quantum properties of, for example, V_{Si} in 4H-SiC are only predominantly available in intrinsic material. Accordingly, controlling the charge state by other means than doping alone is crucial for ensuring optimal emission yield and switching the qubit state ON and OFF at will.

Initially, charge-state control was achieved by optical means via dual excitation. For the NV center in diamond, detection of charge-state switching is simplified by the known optical signals of both the neutral and negative charge states, yielding reliable observation of optically induced charge-state switching between NV^0 and NV^-.[151,152] A comparable mechanism for charge-state switching was recently found for the SnV defect in diamond, where p-i-p structures were used to induce a tunable band bending.[153] The main quantum emitters in SiC on the other hand, V_{Si}, VV, CAV and NV, are each associated with only one bright charge state. Therefore, optical responses to charge-state switching must necessarily be detected based on changes to the color center's emission intensity. Using dual excitation, charge-state control[154,155] and electrometry by optical charge-state conversion[156] were shown for the Si vacancy and divacancy in 4H-SiC. Interestingly, charge-based electric field sensing using optical charge-state switching was subsequently demonstrated using divacancy defects in 4H-SiC.[157]

A drawback of optically induced charge-state switching is the lack of exact control over the Fermi level at which the charge-state transition takes place. Indeed, this complicates verification of and comparison with theoretically predicted charge-state transition levels[39] (see, e.g., refs. [1, 41, 45, 85, 155] for theoretically predicted thermodynamic transition levels for the relevant quantum emitters in SiC). Instead, charge-state transitions can be induced by electrical means via defect integration with devices such as Schottky barrier and p-i-n diodes. Transparent electrodes such as graphene,[158] or alternatively sample backside detection of emission,[42] simplify the preservation of the optical detection mode.

Optically detected and electrically induced charge-state switching of color centers in SiC was first demonstrated for single divacancies by biasing Ti/Au electrodes on a 120 μm thick 4H-SiC membrane.[159] An additional layer of control is provided by knowledge of the sample Fermi level, which can be estimated using device modeling of, for example, p-i-n and Schottky barrier diodes using TCAD simulations. The former strategy was employed for charge-state switching of single divacancies[28] and Si vacancies[160] deposited within the intrinsic layer of the p-i-n diode. Although the color centers can be optically addressed from a variety of directions, their significant distance from the sample surface due to the n and p layers may prove a disadvantage for some applications. Alternatively, Schottky barrier diodes (SBDs) can be employed as shown in ref. [42], and offer faster switching frequencies compared to the p-i-n diode solution combined with near-surface defect control. Other examples of charge-state control over semiconductor color centers include recent demonstrations of charge-state conversion of SiV centers in single-crystal diamond membranes,[161] and charge-state switching of carbon antisite-vacancy pairs in 4H-SiC as detected using electron paramagnetic resonance (EPR).[162]

Consider the example of charge-state control over Si vacancy (V_{Si}) ensembles embedded in n-type 4H-SiC epitaxial layers as obtained using SBDs.[42] **Figure 4**a shows the V1′ emission line originating from $V_{Si}^-(h)$ in two cases: collected from within the depletion region beneath the SBD (purple line), and collected from the same sample but in a region free from the SBD-induced electric field (gray line). Intriguingly, the V1′ emission intensity is enhanced by almost an order of magnitude by the presence of the SBD alone. Sequential application of a forward (reverse) bias to the SBD was further seen to enhance (quench) the V_{Si} ensemble emission (see Figure 4b). Furthermore, ref. [42] combined photoluminescence (PL) measurements, deep level transient spectroscopy (DLTS) and DFT calculations to assign charge-state transitions of V_{Si} to the S1 and S2 DLTS centers,[163] and verify theoretical predictions[41] that the V_{Si}(-/2-) and V_{Si}(2-/3-) transitions occur at 0.7 eV and 0.4 eV below the conduction band edge, respectively[42] (see Figure 1b). Thereby, the model explaining the V_{Si} intensity enhancement (Figure 4a) and modulation (Figure 4b) was constructed, and is summarized by Figure 4c and the following. In n-type material and in the absence of SBDs, V_{Si}^- is not the predominant charge state. Forming an SBD causes band bending near the surface, resulting in an enhanced population of the negatively charged V_{Si} and hence increased emission intensities.

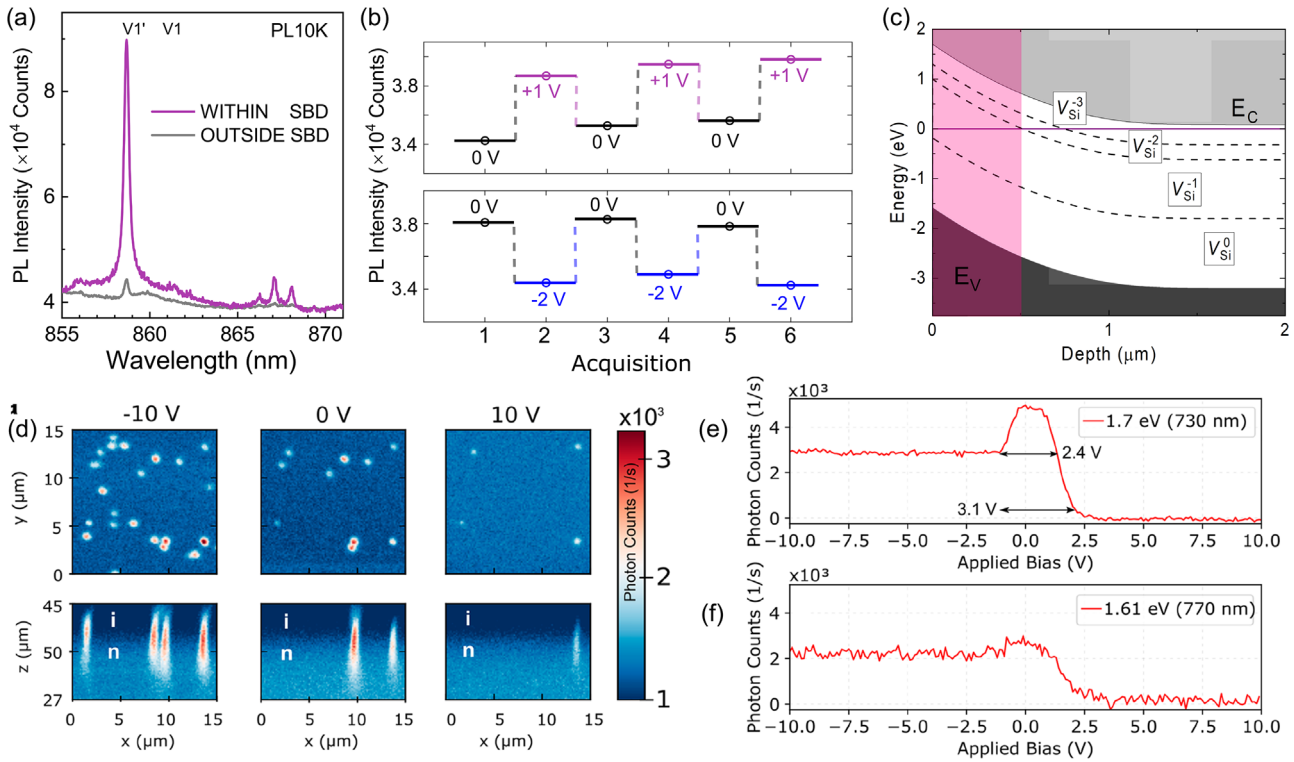

Figure 4. Charge-state control and device integration of quantum emitters in 4H-SiC. a) Influence of electric field from a Schottky barrier diode (SBD) on the V1′ emission line of $V_{Si}^{-}(h)$. b) Charge-state switching of V_{Si} ensembles upon biasing the SBD. c) Influence of SBD-induced electric field on the 4H-SiC band structure and V_{Si}-related defect levels. Panels (a)–(c) are based on data from ref. [42]. d) Electrical charge-state switching of single silicon vacancies shown by confocal scans. e–f) Optical excitation dependence of charge-state conversion, shown by bias-dependent PL intensity curves under different excitation energies. Panels (d)–(f) are reproduced (adapted) with permission.[160] Copyright 2019, American Chemical Society.

It is important to note that some controversy remains regarding interpretation of the charge-state switching models. On one hand, we find the band bending based model for charge-state conversion as presented for V_{Si} in ref. [42] and Figure 4a–c. Other works, such as refs. [154] and [160], invoke the influence of carrier capture and emission from other nearby defect centers to explain the observed emission intensity modulation characteristics. Ref. [160] considers charge-state switching of single V_{Si} centers embedded within the intrinsic region of 4H-SiC p-i-n diodes, as shown in Figure 4d–f. However, as illustrated in Figure 4e and 4f, the switching characteristics depend on the excitation energy. Indeed, under 730 nm excitation the photon count from a single V_{Si} center is enhanced around 0 V applied bias, while this peak was not observed for other excitation conditions, for example, 770 nm as shown in Figure 4f. Due to challenges in explaining this behavior based on band bending alone, ref. [160] discusses a potential mechanism involving capture of charge carriers emitted from nearby V_C defects by V_{Si}. Regardless, further work is needed to fully understand the complex interplay between band bending, defect charge-state transitions and photoluminescence emission.

In addition to the influence on the amount of defects that reside in a specific charge state, electric fields may affect the spin state of the quantum center being probed. For instance, NV^- center spins in diamond are sensitive to electric fields,[164] enabling ultrasensitive and nanoscale electric field sensing.[165] On the other hand, electric field noise may correspondingly cause spin decoherence for the same defect type.[166] In terms of device integration, the electrical degree of freedom has been employed to obtain coherent control over single spins in silicon,[167] drive spin resonance and read-out the spin state of VV[168] and V_{Si} [169] defects in 4H-SiC electrically, and construct a single-photon emitting diode in silicon carbide.[170]

5. Emission Tuning

Having established control over the point defect's formation, thermal stability and charge state via integration with optoelectronic devices, we now turn to direct manipulation of the single-photon emission by external perturbations to the quantum states of a defect emitter, resulting in altered single photon energies. Tuning of the emission energy requires a shifting or splitting of the defect's energy levels, either in the ground or excited states or both. For example, indistinguishable photons were recently obtained in 4H-SiC as shown in ref. [27] by means of magnetic field manipulation, and constitute an important end goal for emission tuning. However, this is not the only reason for manipulating single-photon sources. Tuning the emission energy facilitates selecting the energy specifically for each individual application, and detection of emission energy and intensity changes enables excellent optics-based quantum sensors with nanoscale resolution. Therefore, a broad range of emitters should be studied, and below we discuss electric fields, strain coupling and vibronic

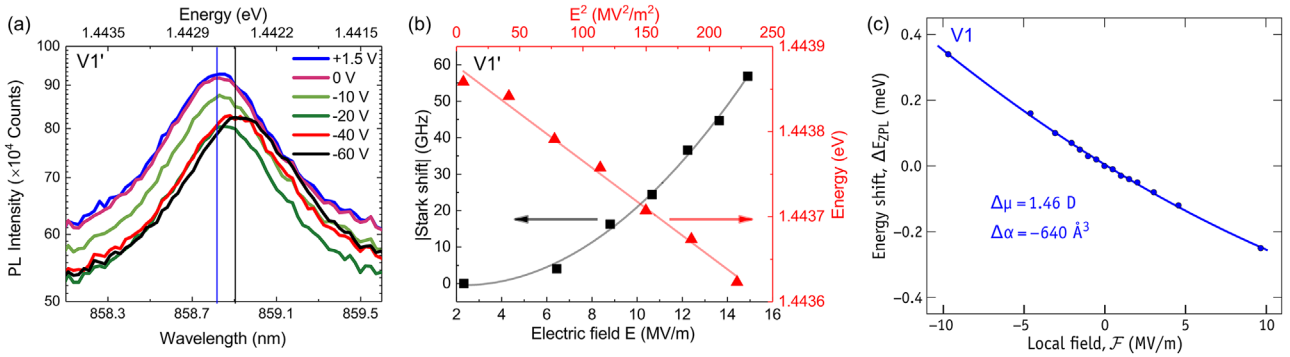

Figure 5. Stark tuning of emission from Si vacancies in 4H-SiC. a,b) Electrically induced shift of the V1′ line attributed to the second excited state of $V_{Si}^{-}(h)$. c) Theoretically predicted Stark shifts of the V1 emission line arising from the first excited state of $V_{Si}^{-}(h)$. Panels (a)–(c) are based on data from refs. [42] and [98], respectively.

effects as potential pathways for externally controlled single-photon emission tuning. Other alternatives include the use of optical pulses for suppressing spectral diffusion[171] and spectral engineering of single photon emission,[172] but will not be discussed further herein.

5.1. Stark Shift of Zero-Phonon Lines

Shifting of emission wavelengths under the application of an electric field is commonly known as the Stark effect.[173] The Stark shift of the zero-phonon line energy (E_{ZPL}) follows the relation[174]

$$\Delta E_{ZPL} = -\Delta\boldsymbol{\mu}\boldsymbol{\mathcal{F}} - \frac{1}{2}\Delta\boldsymbol{\alpha}\boldsymbol{\mathcal{F}}^2 \quad (1)$$

to second order. Here, $\Delta\mu$ and $\Delta\alpha$ (in one dimension) are the respective changes in dipole moment and polarizability between the excited and ground states, and $\boldsymbol{\mathcal{F}}$ is the local field. Strictly linear Stark effects are usually only observed for centrosymmetric defects.[174]

Single NV^- centers in diamond exhibit a rich variety of Stark shifts including linear and quadratic components.[175] Such parabolic dependencies of ΔE_{ZPL} on $\boldsymbol{\mathcal{F}}$ could be explained by field-induced couplings of defect-related and crystalline states.[174] Indeed, ref. [176] applied electric fields along several axes and detected intriguing asymmetries in the NV^- center ZPL shifts, that were attributed to an enhancement and rectification of the local electric field by photoionized charge traps in the material. Interestingly, the SiV center in diamond is a centrosymmetric defect. SiV demonstrates extreme spectral stability deriving from the inversion symmetry,[26] and no Stark shift has been observed, marking SiV centers as highly stable toward stray electric fields. Chromium-based color centers in diamond, on the other hand, display a wide-range electrical tunability of the emission energy.[177]

For the case of 4H-SiC, Stark shifts have been demonstrated for emission from both V_{Si} [42,158] and the divacancy,[28,159] where the divacancy appears to exhibit a quadratic Stark shift. An intriguing application of coupling between the excited states of divacancy spins (in 4H-SiC) to electric fields was shown in ref. [178]. Here, the authors demonstrated electrically driven coherent quantum interference in the zero-phonon line of isolated VV centers, showcasing simultaneous control over the optical and spin degrees of freedom.

The negative charge state of V_{Si} exhibits three zero-phonon lines: V1 and V1′ are attributed to the first and second excited states of $V_{Si}^{-}(h)$, respectively, while V2 was assigned to $V_{Si}^{-}(k)$.[96] The ground and first excited states follow $^4A_2$ symmetry, whereas the second excited states order according to ^4E.[94,95] Ref. [42] reported a pronounced shift for the V1′ ZPL upon application of a bias to SBD devices along the hexagonal crystallographic axis (0001), as illustrated in **Figure 5**a. The Stark effect for V1′ was of a quadratic shape, as shown by Figure 5b. Similar behavior was subsequently demonstrated in ref. [158], but now adding electric fields applied along the crystallographic basal direction as well. Here, the observation of a twofold splitting of the V1′ line nicely accounted for the double degeneracy of the ^4E excited state. A Stark shift was also reported for the V1 ZPL,[158] where approximately linear and quadratic shifts were observed when the applied field was directed along the main axis and parallel to the basal plane, respectively.

It is interesting to quantitatively compare the stability of each defect's ZPL with respect to the electric field. In the case of the NV^- center in diamond, Stark tuning of 10 GHz was obtained in ref. [176], while no Stark shifts have so far been found for SiV. In 4H-SiC, Stark tunabilities for VV by ~800 GHz[28] and V_{Si} by ~60 GHz[42] were found. Although not directly comparable because of different devices, emitter distribution and electric field strengths, these findings indicate a greater field response in SiC compared to that of diamond. Furthermore, we note the seemingly greater sensitivity of VV to stray electric fields than that for V_{Si}. On the other hand, larger Stark shifts may provide greater ease of ensuring photon uniformity and larger emission tunability. Emission tunability is important to select the optimal wavelength for a particular application, and for correcting the discrepancy in emitted photon energies due to inhomogeneous broadening.

Next, we consider the respective changes in polarizability ($\Delta\alpha$) between the excited and ground states of an excited-to-ground state transition, as outlined in Equation (1). Changes in polarizability, $\Delta\alpha'$ ($\Delta\alpha' = 10^{30}\Delta\alpha/4\pi\epsilon_0$), are generally positive and in the 10–100 Å range for quantum dots and molecules.[179,180] The positive polarizabilities can partly be explained by excited

states generally being more polarizable than ground states. Conversely, ref. [175] reported values for $\Delta\alpha'$ between -6×10^4 Å^3 and 0 for NV$^-$ in diamond. The Stark shifts of the V1′ ZPL attributed to $V_{Si}^-(h)$ in 4H-SiC, on the other hand, correspond to $\Delta\alpha' = 4.3 \times 10^3$ Å^3,[42] which is more in keeping with (albeit larger than) reported values for quantum dots and molecules. Note that ref. [158] found a smaller polarizability change of $\Delta\alpha' = 0.17 \times 10^3$ Å^3 for the V1′ transition.

Theoretical studies have proposed methods for computing Stark effects on zero-phonon lines originating from defects embedded in both nano-sized and bulk material based on density functional theory calculations. Previous studies (see, e.g., refs. [140, 181, 182]) have calculated Stark shifts for small molecules and defects in 2D materials like *h*-BN, but corresponding studies for point defects in solids were scarce. This may be related to difficulties arising upon incorporation of macroscopic electric fields[183] in the Hamiltonian, which result in singularities in the charge density that hamper the calculations. One approach for estimating differences in optical dipole moments between ground and excited defect states, and hence linear Stark shifts to E_{ZPL}, combines density-functional perturbation theory and the Berry-phase theory of polarization and was employed in, for example, ref. [184]. However, this method is only applicable for small electric fields (smaller than those applied experimentally in, e.g., ref. [42]), thus leading to minute calculated shifts. Additionally, second- and higher-order effects are challenging to capture at that level of theory. In ref. [98], on the other hand, Stark shifts of defect states in bulk semiconductors were evaluated using 3D periodic boundary conditions and periodic slabs separated by thick vacuum layers, enabling estimates of polarizability changes in addition to dipole moments.

Using the Si vacancy in 4H-SiC as a benchmark system, the electric field dependencies of the V_{Si} optical transitions were estimated theoretically for V1 in ref. [184], and V1 and V2 in ref. [98]. The result for V1 from ref. [98] is illustrated in Figure 5c, and exhibits good qualitative agreement with the experiments of ref. [158]. In the case of the V1 transition and electric fields applied along the *c*-axis (0001) of 4H-SiC, a linear Stark effect with a small $\Delta\alpha'$ and $\Delta\mu = 0.18$ D (1 D = 3.34×10^{-30} Cm) was found.[158] Theoretically, a weak non-linearity with $\Delta\alpha' = -640$ Å^3 was estimated.[98] However, there is a discrepancy between the computed and measured values for $\Delta\mu$ of about a factor of 10, but the computations fall closer to the range found for V1′ ($\Delta\mu \approx 1$ to 2 D)[42,158] and NV$^-$ in diamond ($\Delta\mu$ in the range −1.5 D to 1.5 D).[175] Comparing to the calculations of ref. [184] that yield dipole moment changes for the V1 transition of approximately 0.21 D, greater quantitative agreement in $\Delta\mu$ values is found, but at the expense of higher-order Stark effects.

Discrepancies between theory and experiment may arise due to differences between the estimated electric field used in the calculations and the actual electric field strength affecting the entire distribution of emitters being probed. Variations in polarizability over the ensemble may also arise from differences in orientation and local environment, while differences in the excited-state dipole are largely due to a distribution of dipole orientations relative to the applied field. From the theoretical perspective, numerical instabilities caused by too small supercell or slab size and vacuum thickness must be considered.

Similar theoretical and experimental methodologies as discussed above have been employed for studying Stark tuning of emitters in 2D materials, but the identities of the experimentally detected emitters remain unknown, preventing comparison between theory and experiment. For instance, large Stark shifts have been reported[182,185–187] and predicted[182] for SPEs in *h*-BN, WSe_2,[188] and MoS_2[189] (see **Table 1** for tuning parameters), but the lack of reliable identification of the responsible emitters hinders utilization in quantum devices. Interestingly, the Stark tunability appears larger in 2D materials as compared to, for example, SiC. Another example is the recent demonstration of single-photon emission from interlayer excitons trapped in a $MoSe_2/WSe_2$ heterostructure, where large Stark tunability for the excitons of up to 40 meV was shown.[149]

5.2. Strain Coupling

An alternative to employing external electric fields to tune single-photon emission energies involves utilizing local inhomogeneities. Strain can be applied in several ways, including mechanically compressing the sample and exploiting local stresses arising during growth or processing. For example, strain fields induced by ion tracks have been shown to cause spectral splitting of the zero-phonon line for NV$^-$ centers in diamond,[190] and the strain-sensitive zero-field splitting of NV$^-$ was employed to image stress and magnetism.[191] Furthermore, dynamic strain application to NV$^-$ could mechanically drive coherent spin transitions[192] and mediate coupling of diamond spins to a mechanical resonator.[193] Hence, NV centers in diamond exhibit excellent functionalities for strain sensing, as demonstrated recently by monitoring the ODMR signal of NV center ensembles.[194] **Figure 6** illustrates the potential of NV centers to probe local stress by spatial mapping of the full stress tensor with sub-micrometer resolution.

A proposed application area for strain modification of defect qubits is within quantum information processing (see, e.g., ref. [6]), to for instance coherently couple color centers,[195] reduce spectral diffusion,[196,197] and encode information in isolated defect centers by energy tuning.[195] The coupling between spin and strain has been established theoretically for both NV$^-$ in diamond[198] and divacancies in SiC.[84,199] Indeed, strain tuning via a strain gradient was used to encode information in closely spaced NV$^-$ centers in diamond,[195] and proposed to enable control over optical resonance between two SiV centers in diamond.[197]

Returning to the example of V_{Si} and VV emitters in SiC, strain was early on proposed to affect emission from the Si vacancy in 4H and 6H SiC.[93] Theory predicts that strain couples strongly to defect energy levels in SiC. Theoretically predicted shifts in the ZPL energy for V_{Si} [97] and $V_{Si}V_C$ [199,200] due to strain are in the range of several meV, exceeding that achieved via Stark tuning.[28,42,158,159]

A recent study focused on Si vacancies embedded in 6H-SiC microparticles (see **Figure 7**a). As shown by the cathodoluminescence (CL) color maps in Figures 7b,c, significant shifts of the V1, V2, and V3 emission lines (assigned to V_{Si}^- in 6H-SiC[99]) were found depending on the emitter localization across the sample. In Figure 7d the ZPL shifts were revealed to be up to 8–26 meV

Table 1. Manipulation parameters of relevant materials (host) and point defect emitters, including bright charge state (q) and stable Fermi level (E_F) range above the valence band edge E_V, spin coherence time (T_2), single-photon emission ZPL energy (ZPL), emission brightness (Brightn.), emission purity $g^{(2)}(0)$, Debye-Waller factor (DWF), Stark tuning (Stark) and strain tuning (Strain).

Host	Defect[q]	E_F-range [eV]	T_2 [ms]	ZPL [nm]	Brightn. [Hz]	$g^{(2)}(0)$	DWF (%)	Stark [meV]	Strain [meV]
C	NV^-	2.7–5.0	2 (RT)[22]	637[61]	10^6[226]	0.1[226]	3-5	0.04[176]	0.4[195]
C	SiV^-	1.4–2.1[82]	0.04 (4 K)[75]	738[73]	10^6[73]	0.1[73]	70[21]		0.37[197]
C	GeV^-	1.9–2.7[82]	0.1 (5 K)[81]	602[80]		0.05[80]	70 [80]		
SiC	V_{Si}^-	1.2–2.5[41,42]	20 (17 K)[227]	858–916[94]	10^4[52]	0.25[27]	6–9[97]	3[158]	26[201]
SiC	$V_{Si}V_C^0$	1.2–2.3[44]	64 (5 K)[117]	1078–1134[84]	10^5[56]	0.06[56]	3–6[56]	2.5[28]	
SiC	$C_{Si}V_C^+$	1.3–2.2[45]		640–680[87]	10^6[87]	0.1[87]			
h-BN				560–780[132]	10^6[228]	0.08[229]	81[134]	15 [185]	65 [202]
WSe_2				730–750[132]		0.12[204]		21[230]	18[204]

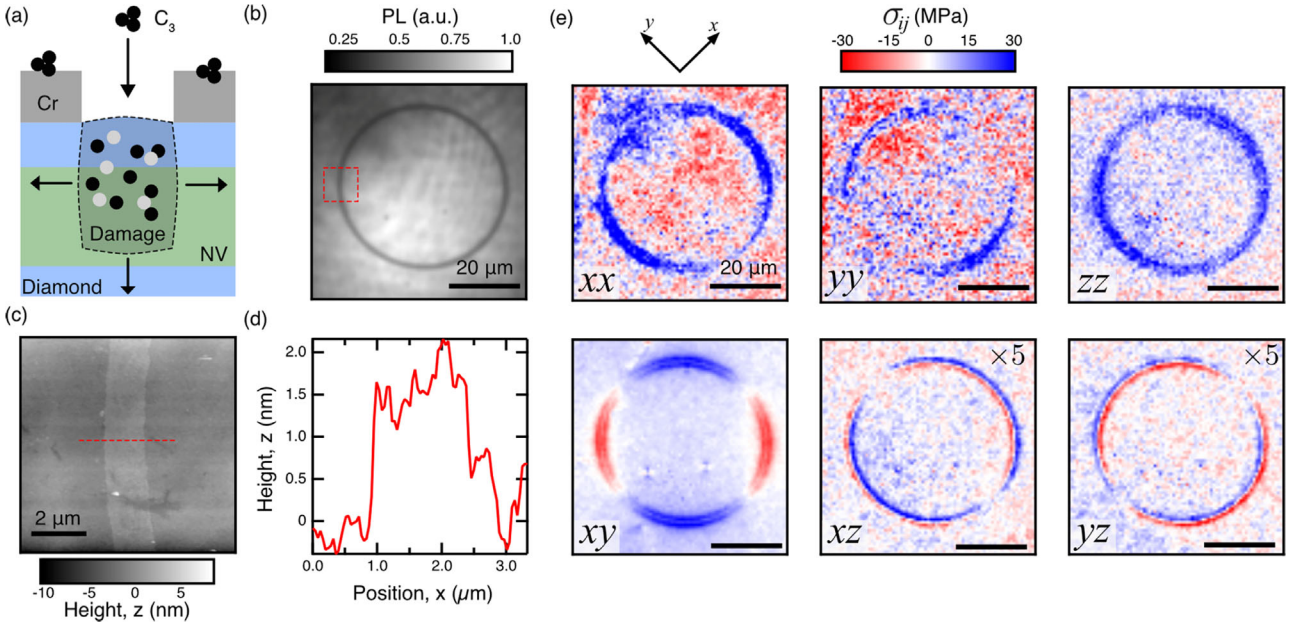

Figure 6. Stress imaging using NV centers in diamond. a–d) Stress is induced by locally implanting C_3 molecules, and e) the six stress tensor components are imaged by measuring the NV sensors. Reproduced with permission.[194] Copyright 2019, American Chemical Society.

in size, and attributed to basal compressive strain of 2.3% along the particle a-direction ($11\bar{2}0$) by geometric phase analysis (GPA) as implemented in transmission electron microscopy (TEM).[201] A strain coupling parameter of 1.13 eV per strain was estimated for the largest ZPL shifts, in excellent agreement with theoretical predictions of 1–2 eV/strain coupling constants along the basal plane for V_{Si} emitters in 4H-SiC.[97] The same study predicted even larger strain coupling parameters in the 6–7 eV per strain range along the axial (0001) direction, foreshadowing larger ZPL shifts for different sample types.

Importantly, strain-induced ZPL shifts in the 20–30 meV range[201] far exceed the emission tuning of 1–3 meV achieved by electric field modification of SiC emitters.[28,42,158] Thus, local strain variations can have a potentially detrimental impact on photon indistinguishability, with emitted energies being closely related to local matrix variations. On the other hand, strain tuning also arises as a promising pathway for combating spectral diffusion caused by stray electric fields from local charge variations on single photon energies.

Considering the case of emerging materials, strain was recently used to modify optical characteristics of quantum emitters in h-BN.[202] Indeed, tuning magnitudes of up to 65 meV were achieved, exceeding that shown for, for example, the Si vacancy in SiC.[201] Although reliable identification of the defect emitters is missing, a recent theoretical work suggested that the nitrogen antisite-vacancy pair ($N_B V_N$) in h-BN exhibits large strain-coupling constants of up to 12 eV per strain[203]—double of that predicted for Si vacancies in 4H-SiC.[97] Continuing the consideration of 2D materials, quantum light sources in transition metal dichalcogenides (TMDCs) show intriguing responses to strain manipulation. In ref. [143], a 2D lattice of quantum emitters was constructed in atomically thin WSe_2 via the creation of point-like strain perturbations. Furthermore, strain fields exerted by a piezoelectric device were capable of tuning single-photon

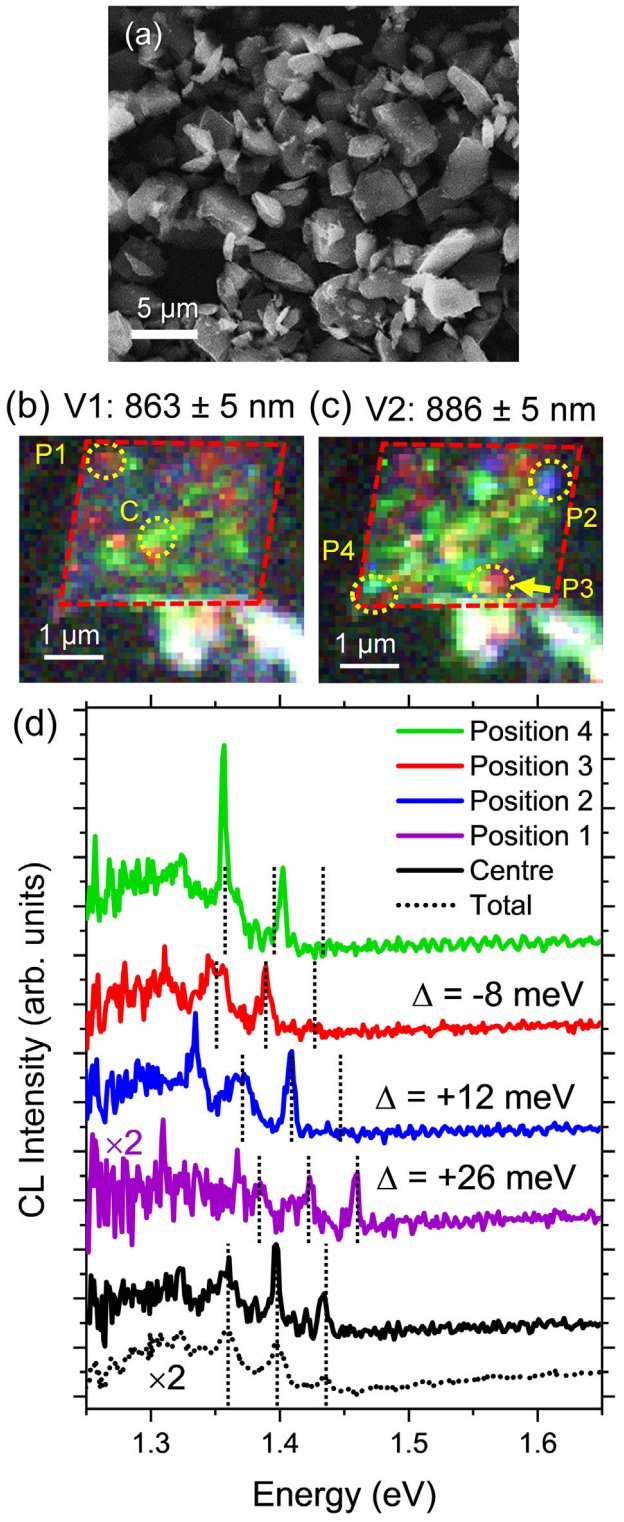

Figure 7. Strain tuning of emission from Si vacancies in 6H-SiC microparticles. a) SEM micrograph of the 6H-SiC microparticles. b,c) False cathodoluminescence (CL) color maps showing emitter localization. d) CL spectra collected from the regions marked in (b) and (c) and revealing strain-induced emission shifting. Reproduced with permission.[201] Copyright 2020, American Chemical Society.

emission energies of localized excitons in WSe_2 by up to 18 meV.[204] To conclude, strain emerges as a highly promising means of emitter control, with the unidentified and strain-susceptible light sources in 2D materials being deserving of further attention.

5.3. Vibronic Effects

Quantum emitters couple to lattice vibrations, resulting in broad phonon side-bands (PSBs) accompanying the sharp zero-phonon lines (ZPLs). The Debye-Waller factor representing the amount of emission channeled into the ZPL varies from 3–5% for NV^- in diamond and 7–9% for V_{Si} and VV in SiC, to around 70% for the centrosymmetric SiV and GeV centers in diamond. In comparison, single-photon emitters in, for example, *h*-BN have been reported to exhibit DWFs of up to 81%.[134] An example PL spectrum showcasing the interplay between sharp ZPLs (V1′, V1 and V2) and broad and overlapping phonon replicas is shown in **Figure 8**a for V_{Si} in n-type 4H-SiC. Understanding the coupling of a quantum emitter to lattice vibrations is thus important to fully identify a defect's fingerprint, but also to maintain control over the emission process and combat the detrimental influence of electron-phonon coupling on photon indistinguishability.

Theoretical studies based on DFT calculations have been utilized to predict and understand vibronic coupling to defect states. A convenient approach to estimate vibrational energies and Franck-Condon relaxation energies is using configuration coordinate (CC) diagrams,[39,205] as shown schematically in Figure 8b. In the case of strong electron-phonon coupling, such as the case for optical charge-state transitions in materials like ZnO, defect-induced local vibrational modes (LVMs) are sufficient to compute defect-related photoluminescence lineshapes.[206] However, the quantum emitters discussed herein more frequently exhibit weak or intermediate electron-phonon coupling, exhibiting sharp ZPLs and a spectrum of phonon satellites. In that case, bulk phonons must also be incorporated to estimate the full emission spectrum including phonon replicas.

The full emission spectra from SPEs in diamond were computed and compared to experiment in ref. [65] for NV^-, and ref. [82] for SiV and GeV. Recent theoretical works have performed comparable studies for Si vacancy emitters in 4H-SiC, by computing photoluminescence lineshapes,[207] estimating the geometry and energy of local vibrational modes (LVMs),[207,208] and discussing the effect of vibronic states on the temperature and strain dependence of V_{Si} qubits.[97] For instance, refs. [207, 208] evaluated the closest local vibrational modes of the V1 and V2 centers at least ~35 meV away from the relevant zero-phonon lines.

An intriguing outcome of electron-phonon coupling was examined and utilized in ref. [209], where a surface-acoustic wave (SAW) resonator was coupled to a superconducting qubit, and the qubit was used to control quantum states in the mechanical resonator. Indeed, the qubits then offer control over mechanical degrees of freedom by coupling to phonon modes. A potential application area for such devices would be to couple stationary qubits to flying ones in the form of phonons. Coupling of spins to mechanics has been shown for, for example, the NV center in diamond, via coherent control[210] and mechanical driving[192] of

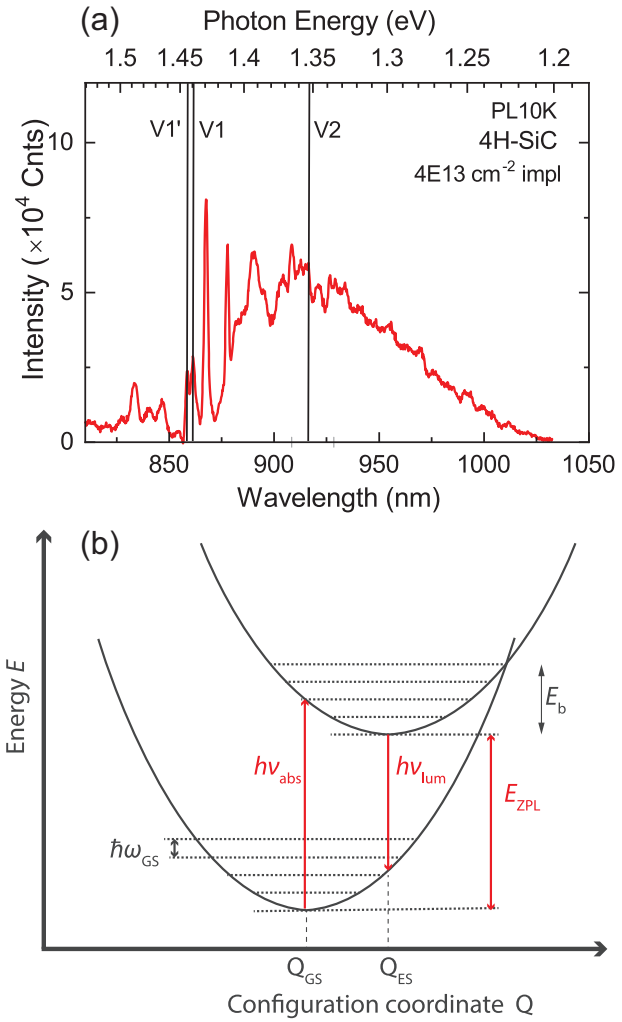

Figure 8. Vibronic effects and single-photon emission. a) Example photoluminescence (PL) spectrum from a proton-irradiated 4H-SiC sample illustrating the broad phonon side-bands surrounding the V1′, V1 and V2 zero-phonon lines of V_{Si}^{-}. Based on data from ref. [42]. b) Conceptual configuration coordinate (CC) diagram for a defect-related transition.

the electron spin localized at NV^{-}. As mentioned above, strain can drive electron spins, and SAW devices are capable of generating the necessary dynamic strain. Indeed, ref. [211] demonstrated acoustically driven spin transitions for divacancy defect ensembles in 4H-SiC via both uniaxial and shear strains, as applied using a Gaussian SAW phonon resonator.

6. Coupling to Photonic Devices

Photonic devices can enhance the directionality and emission rate of single-photon emission from quantum defects embedded within the device. Herein, we discuss two types of photonic devices: passive devices (e.g., waveguides) that augment the collection efficiency by directionalizing the emission, and active devices that enhance the emission rate of the color center (e.g., cavities via the Purcell effect). See, e.g., ref. [32] for a more detailed discussion.

Above, we have discussed integration of quantum emitters in opto-electronic devices such as SBDs, p-i-n diodes and light emitting diodes (LEDs), which has been accomplished for SPEs in both diamond[212–215] and 4H-SiC.[28,42,159,160,169,216] The opto-electronic devices employ electric fields to, for example, stimulate light emission, enhance or diminish emission intensity, and shift the emission energy. Waveguide devices, on the other hand, aim to directionalize the emission in order to ensure maximum collection. In SiC, solid immersion lenses (SILs) that are milled into the substrate and contain one or more quantum emitters have become popular,[52] and strategies for large-scale fabrication have been proposed.[217] **Figure 9**a illustrates a SIL milled into a 4H-SiC wafer (top) and single V_{Si} defects embedded therein (bottom), demonstrating the potential of the SIL platform for detecting isolated emitters. Alternatively, suspended waveguides[218] or arrays of nanopillars containing single emission centers[219] provide similar capabilities but promise greater ease of fabrication, while ref. [220] demonstrated depressed-cladding waveguides written by femtosecond laser in 6H-SiC. The nanopillar waveguide platform is depicted in Figure 9b,c, while the nanopillar array and the single emitters they contain are shown in Figure 9d. Furthermore, ref. [201] discusses the potential of utilizing naturally formed 6H-SiC microcrystals and their individual morphologies for waveguiding purposes, and SiC nanoparticles[221] could be employed in a similar context. In the case of diamond, the quest for ensuring high-yield emission recently reached an important milestone, via fabrication of diamond waveguide arrays containing highly coherent color centers (SiV and GeV) on a photonic integrated circuit.[222]

Cavities couple to the emitter and enhance the emission rate via the Purcell effect. Indeed, cavity coupling is capable of altering the density of final states, meaning that emitters coupled to cavity modes can exhibit both enhanced emission brightness and a larger portion of emission channeled into the zero-phonon line (i.e., larger Debye-Waller factor). For instance, single SiV emitters in diamond were coupled to monolithic optical cavities, resulting in 10-fold lifetime reduction and an enhancement in emission intensity by a factor of 42.[223] SiV centers already exhibit DW factors around 70%, but in the case of NV centers in diamond, cavity coupling enhanced the emission intensity and increased the ZPL branching ratio from 3–5% to around 25%,[224] and later the ZPL transition rate was enhanced by a factor of 70.[225]

Table 1 summarizes key parameters for prominent quantum emitters discussed herein: the NV, SiV and GeV centers in diamond, V_{Si}, VV and CAV in SiC, and unidentified emitters in *h*-BN and WSe_2. Brightness is a key specification for functionalization of SPEs for, fo example, optical quantum computers and quantum repeaters, and is quoted in Table 1. Emitter brightness has been shown to exceed 10^6 kCounts s^{-1} for several defect candidates, but is restricted to one or two orders of magnitude lower values in the case of VV and V_{Si} in SiC. Importantly, although the solitary V_{Si} in SiC exhibits a relatively low count rate of 3–5 kCounts s^{-1}, the fluorescence brightness can be enhanced to 40–50 kCounts s^{-1} using, for example, solid immersion lenses.[52] In comparison, self-assembled InGaAs quantum dots have been shown to reach brightness levels exceeding 10^7 Hz with simultaneous single-photon emission purity values of $g^{(2)}(0) \approx 0.01$.[231]

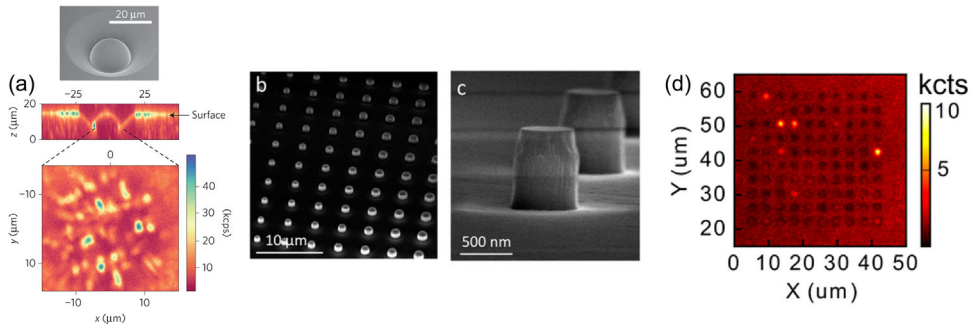

Figure 9. Coupling of quantum emitters to photonic devices in 4H-SiC. a) Solid-immersion lens (top) and localized V_{Si} emitters embedded therein (bottom). b,c) Array of nanopillar waveguides, and d) focused emission from single V_{Si} centers embedded within the array of nanopillars. Panel (a) is reproduced with permission.[52] Copyright 2015, Springer Nature. Panels (b)–(d) are reproduced with permission[219] Copyright 2017, American Chemical Society.

Diamond hosts centrosymmetric SPEs (e.g., SiV and GeV) that facilitate high ZPL branching ratios even in the absence of cavities and resonators. However, as discussed above, spin coherence times in the ms range are only available at temperatures below 1 K in the case of SiV and GeV. Defects in SiC, on the other hand, combine higher-temperature operation with ZPL branching ratios exceeding that of NV^- in diamond. Regardless, coupling of SiC emitters to resonators and cavities[232] is likely necessary in order to realize quantum repeaters, due to the relatively low Debye-Waller factors below 10%. Purcell enhancement via cavity coupling was demonstrated for V_{Si} [233–235] and VV[236] in 4H-SiC, resulting in drastically augmented DW factors of ~50% for V_{Si} [233] and ~75% for $V_{Si}V_C$.[236] Comparing SiC and diamond, cavities were found to enhance the diamond NV and SiV defect emission by up to 70 times, while enhancement of up to a factor of 120 was demonstrated in SiC for V_{Si} and VV.[32] Indeed, this observation indicates the advantage of SiC over diamond in terms of fabrication maturity.

An important factor in terms of integration with photonic devices is related to device fabrication. A more detailed comparison between diamond and SiC fabrication technologies is available in, for example, refs. [14, 32], but we will include a short discussion herein. Several material properties mark the differences between SiC and diamond. The larger band gap of diamond enables a greater transparency window, but doping of SiC is more mature than for diamond, ensuring ease of fabrication of, for example, p-i-n and MOS devices. Passive photonic devices (e.g., solid immersion lenses and nanopillars) can be scalably manufactured and are capable of enhancing collection efficiencies in both diamond and SiC (see, e.g., refs. [217, 219]). Fabrication of microresonators is available in both SiC and diamond with comparable quality,[232,237] while photonic crystal nanocavities can be created with larger variety and quality in SiC because of the more versatile thin-film platform.[238,239] Importantly, nanostructures can have a detrimental impact on spectral stability and broaden emission linewidths, an effect that is less pronounced for centrosymmetric defects[14]—which are not available in, for example, 4H-SiC. Surface passivation could be an approach to mitigate spectral diffusion caused by device integration, but further research is needed to control the response of the different defects.

For alternative material platforms, several recent advances highlight the promise of additional point defect hosts besides diamond and SiC. For instance, Purcell enhancement of spontaneous emission rates for SPEs in GaAsN (related to individual nitrogen luminescence centers) was achieved by fabrication of 2D crystal slabs, resulting in a Purcell factor of 6.3.[240] Color centers in 2D *h*-BN have been coupled to an optical fiber, yielding 10% coupling efficiencies and exemplifying a fully fiber integrated system.[241] Furthermore, emitters hosted by *h*-BN have been successfully coupled to cavities[242] and Purcell enhancement was shown for emitters in WSe_2 with a factor of ~16,[243] heralding a new era in quantum photonics with 2D materials.

7. Perspective on Emitter Manipulation

The wide range of quantum compatible properties summarized in Table 1 indicates that the choice of emitter could end up strongly depending on the application. For instance, single-photon emission purity (as characterized by $g^{(2)}(0)$) may vary strongly between different materials, and even between different color centers within the same material platform (e.g., SiC). As mentioned above, point defect emitters have still not reached purity levels exceeding 99% ($g^{(2)}(0) < 0.01$), which have been demonstrated for, for example, InGaAs quantum dots.[16] Thus, understanding the electronic structure of each point defect emitter and the mechanism behind decoherence and spectral broadening, in addition to developing methods for enhancing or suppressing the various interactions with the defect's environment—that is, via SPE tuning—is vital for the successful integration of point defect based color centers with quantum technologies.

Comparing the various point defect candidates (see Table 1), diamond holds one major advantage over the other materials: the presence of centrosymmetry, enabling defect centers with inversion symmetry such as SiV and GeV. Importantly, as shown for SiV,[26] these defect emitters can facilitate indistinguishable photon emission with 70% of emission being channeled into the ZPL. Moreover, inversion symmetry is associated with greater stability toward external perturbations such as electric fields and strain, a trend that is supported by the parameters in Table 1. Unfortunately, spin coherence times for SiV and GeV are low (in contrast to that for NV), impeding combined utilization as optically controlled spin qubits. Therefore, diamond emitters remain the frontrunner on account of the potential for inversion symmetry, but both V_{Si} and VV in SiC are stronger candidates for spin-photon entanglement than, for example, SiV and GeV,

while simultaneously challenging the NV center in terms of SPE parameters. In fact, the emission from diamond color centers in the visible range is not ideally compatible with fiber optic technology, in contrast to the divacancy and NV emission in SiC at telecom wavelengths. Additionally, it should be noted that the greater potential for single-photon emission tunability may prove an advantage for host materials such as SiC, *h*-BN and WSe_2.

Control of point defect emission will be essential for successful utilization in quantum sensors and communication technologies. Charge-state identification is the first step along the way, as optimal emission yield can only be achieved after the stability range of the bright state is obtained. In this respect, the centrosymmetric defects in diamond (SiV and GeV) are at a slight disadvantage compared to, for example, NV^- and the SiC defects, having a smaller Fermi level range where the negative charge state is stable (although there have been investigations into utilizing the neutral configurations instead). However, to exploit this knowledge to enhance and control emission as exemplified in refs. [28,42,160], the ability to manipulate energy band bending is beneficial. Indeed, the charge-depleted environment in SiC p-i-n diodes was even shown to reduce spectral diffusion toward the lifetime limit.[28] The varied doping protocols and ease of fabrication for SiC, as compared to diamond and the 2D materials, point toward more straightforward managing of the emitter charge state and environment.

Tuning of single-photon emission is a tool for combating spectral diffusion, encoding information in the optical transitions of point defects and attuning the photon energy to specific applications. A common trend for SiC and diamond seems to be that strain tuning yields larger emission modulation than that induced by the electric field (see Table 1), while one of the 2D materials (WSe_2) deviates from this pattern. Interestingly, even though the centrosymmetric SiV center in diamond has so far been found unresponsive to Stark shifts, the SiV^- ZPL is still sensitive to strain. Undoubtedly, several aspects of the complex interplay between quantum emitters and their surroundings remain uncharted. Both important sources for spectral diffusion and optimal cavity coupling strategies must likely be identified to approach the required brightness, purity and indistinguishability parameters for utilization of point defect SPEs in quantum communication applications.

8. Concluding Remarks

To summarize, recent progress related to manipulation of point defects in semiconductors used as single-photon sources for quantum computing, communication and sensing applications is discussed, with a particular emphasis on silicon carbide. Diamond has been a popular color center host for several decades, but silicon carbide is emerging as a front runner due to its tantalizing combination of low spin-orbit and moderate electron-phonon coupling with advanced and mature fabrication and processing. With charge-state control and indistinguishable single-photon emission being established, combined with the recent achievement of 4H-silicon-carbide-on-insulator resonators, SiC emitters are poised for strategic device integration.

Further work in several areas is needed for the successful utilization of point defect SPEs in quantum devices. For instance, the intriguing interplay between temperature, spin coherence, phonon interactions and coupling to cavity devices should be further explored, enabling advanced sensing devices and long-range communication. Moreover, although single-photon emission tuning via external manipulation (e.g., magnetic, electric, and strain fields) has been shown, studies on the combined influence of these effects and their relative strengths remain scarce. Finally, several promising materials such as Si and *h*-BN are on the verge of successful defect identification and charge-state control toward SPE and qubit utilization, which would place these new contenders firmly in the race for quantum applications.

Acknowledgements

Financial support was kindly provided by the Research Council of Norway and the University of Oslo through the frontier research project FUNDAMeNT (No. 251131, FriPro ToppForsk-program). The Research Council of Norway is acknowledged for the support to the Norwegian Micro- and Nano-Fabrication Facility, NorFab, project number 295864.

Conflict of Interest

The authors declare no conflict of interest.

Keywords

electric fields, point defects, quantum technology, single-photon emission, strain, vibronic effects

Received: January 11, 2021
Revised: May 3, 2021
Published online: May 24, 2021

[1] J. R. Weber, W. F. Koehl, J. B. Varley, A. Janotti, B. B. Buckley, C. G. Van de Walle, D. D. Awschalom, *Proc. Natl. Acad. Sci. USA* **2010**, *107*, 8513.
[2] D. D. Awschalom, R. Hanson, J. Wrachtrup, B. B. Zhou, *Nat. Photonics* **2018**, *12*, 516.
[3] V. Acosta, P. Hemmer, *MRS Bull.* **2013**, *38*, 127.
[4] I. Aharonovich, D. Englund, M. Toth, *Nat. Photonics* **2016**, *10*, 631.
[5] L. Rondin, L.-P. Tetienne, T. Hingant, J.-F. Roch, P. Maletinsky, V. Jacques, *Rep. Prog. Phys.* **2014**, *77*, 056503.
[6] G. Wolfowicz, F. J. Heremans, C. P. Anderson, S. Kanai, H. Seo, A. Gali, G. Galli, D. D. Awschalom, *Nat. Rev. Mater.* **2021**, https://doi.org/10.1038/s41578-021-00306-y.
[7] D. P. DiVincenzo, *Fortschr. Phys.* **2000**, *48*, 771.
[8] T. D. Ladd, F. Jelezko, R. Laflamme, Y. Nakamura, C. Monroe, J. L. O'Brien, *Nature* **2010**, *464*, 45.
[9] J. L. O'Brien, *Science* **2007**, *318*, 1567.
[10] N. Gisin, G. Ribordy, W. Tittel, H. Zbinden, *Rev. Mod. Phys.* **2002**, *74*, 145.
[11] N. Gisin, R. Thew, *Nat. Photonics* **2007**, *1*, 165.
[12] W. J. Munro, K. Azuma, K. Tamaki, K. Nemoto, *IEEE J. Sel. Top. Quantum Electron.* **2015**, *21*, 6400813.
[13] S. Buckley, K. Rivoire, J. Vucković, *Rep. Prog. Phys.* **2012**, *75*, 126503.
[14] D. M. Lukin, M. A. Guidry, J. Vucković, *PRX Quantum* **2020**, *1*, 020102.
[15] C. K. Hong, Z. Y. Ou, L. Mandel, *Phys. Rev. Lett.* **1987**, *59*, 2044.
[16] N. Somaschi, V. Giesz, L. de Santis, J. C. Loredo, M. P. Almeida, G. Hornecker, S. L. Portalupi, T. Grange, C. Anton, J. Demory, C. Gomez, I. Sagnes, N. D. Lanzillotti Kimura, A. Lemaitre, A. Auffeves, A. G. White, L. Lanco, P. Senellart, *Nat. Photonics* **2016**, *10*, 340.

[17] J. Liu, R. Su, Y. Wei, B. Yao, S. F. Covre da Silva, Y. Yu, J. Iles-Smith, K. Srinivasan, A. Rastelli, J. Li, X. Wang, *Nat. Nanotechnol.* **2019**, *14*, 586.
[18] N. Tomm, A. Javadi, N. O. Antoniadis, D. Najer, M. C. Löbl, A. R. Korsch, R. Schott, S. R. Valentin, A. D. Wieck, A. Ludwig, R. J. Warburton, *Nat. Nanotechnol.* **2021**.
[19] M. W. Doherty, N. B. Manson, P. Delaney, L. C. L. Hollenberg, *New J. Phys.* **2011**, *13*, 025019.
[20] M. W. Doherty, N. B. Manson, P. Delaney, F. Jelezko, J. Wrachtrup, L. C. L. Hollenberg, *Phys. Rep.* **2013**, *528*, 1.
[21] I. Aharonovich, S. Castelletto, D. A. Simpson, C.-H. Su, A. D. Greentree, S. Prawer, *Rep. Prog. Phys.* **2011**, *74*, 076501.
[22] G. Balasubramanian, P. Neumann, D. Twitchen, M. Markham, R. Kolesov, N. Mizuochi, J. Isoya, J. Achard, J. Beck, J. Tissler, V. Jacques, P. R. Hemmer, F. Jelezko, J. Wrachtrup, *Nat. Mater.* **2009**, *8*, 383.
[23] G. Balasubramanian, I. Y. Chan, R. Kolesov, M. Al-Hmoud, J. Tisler, C. Shin, C. Kim, A. Wojcik, P. R. Hemmer, A. Krueger, T. Hanke, A. Leitenstorfer, R. Bratschitsch, F. Jelezko, J. Wrachtrup, *Nature* **2008**, *455*, 648.
[24] D. Le Sage, L. Arai, D. R. Glenn, S. J. DeVience, L. M. Pham, L. Rahn-Lee, M. D. Lukin, A. Yacoby, A. Komeili, R. L. Walsworth, *Nature* **2013**, *496*, 486.
[25] J. T. Muhonen, J. P. Dehollain, A. Laucht, F. E. Hudson, R. Kalra, T. Sekiguchi, K. M. Itoh, D. N. Jamieson, J. C. McCallum, A. S. Dzurak, A. Morello, *Nat. Nanotechnol.* **2014**, *9*, 986.
[26] A. Sipahigil, K. D. Lanke, L. J. Rogers, T. Teraji, J. Isoya, A. S. Zibrov, F. Jelezko, M. D. Lukin, *Phys. Rev. Lett.* **2014**, *113*, 113602.
[27] N. Morioka, C. Babin, R. Nagy, I. Gediz, E. Hesselmeier, D. Liu, M. Joliffe, M. Niethammer, D. Dasari, V. Vorobyov, R. Kolesov, R. Stöhr, J. Ul Hassan, N. T. Son, T. Ohshima, P. Udvarhelyi, G. Thiering, A. Gali, J. Wrachtrup, F. Kaiser, *Nat. Commun.* **2020**, *11*, 2516.
[28] C. P. Anderson, A. Bourassa, K. C. Miao, G. Wolfowicz, P. J. Mintun, A. L. Crook, H. Abe, J. Ul Hassan, N. T. Son, T. Oshima, D. D. Awschalom, *Science* **2019**, *366*, 1225.
[29] B. Lounis, M. Orrit, *Rep. Prog. Phys.* **2005**, *68*, 1129.
[30] M. Atatüre, D. Englund, N. Vamivakas, S.-Y. Lee, J. Wrachtrup, *Nat. Rev. Mater.* **2018**, *3*, 38.
[31] L. C. Bassett, A. Alkauskas, A. L. Exarhos, K.-M. C. Fu, *Nanophotonics* **2019**, *8*, 1867.
[32] V. A. Norman, S. Majety, Z. Wang, W. H. Casey, N. Curro, M. Radulaski, *InfoMat* **2020**, https://doi.org/10.1002/inf2.12128.
[33] G. Zhang, Y. Cheng, J.-P. Chou, A. Gali, *Appl. Phys. Rev.* **2020**, *7*, 031308.
[34] N. T. Son, C. P. Anderson, A. Bourassa, K. C. Miao, C. Babin, M. Widmann, M. Niethammer, J. Ul Hassan, N. Morioka, I. G. Ivanov, F. Kaiser, J. Wrachtrup, D. D. Awschalom, *Appl. Phys. Lett.* **2020**, *116*, 190501.
[35] S. Castelletto, A. Boretti, *J. Phys.: Photonics* **2020**, *2*, 022001.
[36] I. Aharonovich, E. Neu, *Adv. Opt. Mater.* **2014**, *2*, 911.
[37] M. Radulaski, J. L. Zhang, Y.-K. Tzeng, K. G. Lagoudakis, H. Ishiwata, C. Dory, K. A. Fischer, Y. A. Kelaita, S. Sun, P. C. Maurer, K. Alassaad, G. Ferro, Z.-X. Shen, N. A. Melosh, S. Chu, J. Vučković, *Laser Photon. Rev.* **2019**, *13*, 1800316.
[38] C. Bradac, W. Gao, J. Forneris, M. E. Trusheim, I. Aharonovich, *Nat. Commun.* **2019**, *10*, 5625.
[39] C. Freysoldt, B. Grabowski, T. Hickel, , J. Neugebauer, *Rev. Mod. Phys.* **2014**, *86*, 253.
[40] C. E. Dreyer, A. Alkauskas, J. L. Lyons, A. Janotti, C. G. Van de Walle, *Annu. Rev. Mater. Res.* **2018**, *48*, 1.
[41] T. Hornos, A. Gali, B. G. Svensson, *Mater. Sci. Forum* **2011**, *679–680*, 261.
[42] M. E. Bathen, A. Galeckas, J. Müting, H. M. Ayedh, U. Grossner, J. Coutinho, Y. K. Frodason, L. Vines, *npj Quantum Inf.* **2019**, *5*, 111.
[43] J. Coutinho, V. J. B. Torres, K. Demmouche, S. Öberg, *Phys. Rev. B* **2017**, *96*, 174105.
[44] A. Beste, D. E. Taylor, D. A. Golter, C. W. Lai, *Phys. Rev. B* **2018**, *98*, 214107.
[45] K. Szász, V. Ivády, I. A. Abrikosov, E. Janzén, M. Bockstedte, A. Gali, *Phys. Rev. B* **2015**, *91*, 121201(R).
[46] A. Csóré, H. J. von Bardeleben, J. L. Cantin, A. Gali, *Phys. Rev. B* **2017**, *96*, 085204.
[47] K. F. Dombrowski, U. Kaufmann, M. Kunzer, K. Maier, J. Schneider, *Appl. Phys. Lett.* **1994**, *65*, 1811.
[48] G. Wolfowicz, C. P. Anderson, B. Diler, O. G. Poluektov, F. J. Heremans, D. D. Awschalom, *Sci. Adv.* **2020**, *6*, eaaz1192.
[49] H. J. von Bardeleben, J. L. Cantin, A. Csóré, A. Gali, E. Rauls, U. Gerstmann, *Phys. Rev. B* **2016**, *94*, 121202(R).
[50] I. Pelant, J. Valenta, *Luminescence Spectroscopy of Semiconductors*, Oxford University Press, Oxford, UK **2012**.
[51] N. T. Son, X. T. Trinh, L. S. Løvlie, B. G. Svensson, K. Kawahara, J. Suda, T. Kimoto, T. Umeda, J. Isoya, T. Makino, T. Ohshima, E. Janzén, *Phys. Rev. Lett.* **2012**, *109*, 187603.
[52] M. Widmann, S.-Y. Lee, T. Rendler, N. T. Son, H. Fedder, S. Paik, L.-P. Yang, N. Zhao, S. Yang, I. Booker, A. Denisenko, M. Jamali, S. A. Momenzadeh, I. Gerhardt, T. Ohshima, A. Gali, E. Janzén, J. Wrachtrup, *Nat. Mater.* **2015**, *14*, 164.
[53] P. Lodahl, S. Mahmoodian, S. Stobbe, *Rev. Mod. Phys.* **2015**, *87*, 347.
[54] M. Bayer, A. Forchel, *Phys. Rev. B* **2002**, *65*, 041308(R).
[55] A. V. Kuhlmann, J. H. Prechtel, J. Houel, A. Ludwig, D. Reuter, A. D. Wieck, R. J. Warburton, *Nat. Commun.* **2015**, *6*, 8204.
[56] D. J. Christle, P. V. Klimov, C. F. de las Casas, K. Szász, V. Ivády, V. Jokubavicius, J. Ul Hassan, M. Syväjärvi, W. F. Koehl, T. Ohshima, N. T. Son, E. Janzén, A. Gali, D. D. Awschalom, *Phys. Rev. X* **2017**, *7*, 021046.
[57] H. Kraus, D. Simin, C. Kasper, Y. Suda, S. Kawabata, W. Kada, T. Honda, Y. Hijikata, T. Ohshima, V. Dyakonov, G. V. Astakhov, *Nano Lett.* **2017**, *17*, 2865.
[58] Y.-C. Chen, P. S. Salter, S. Knauer, L. Weng, A. C. Frangeskou, C. J. Stephen, S. N. Ishmael, P. R. Dolan, S. Johnson, B. L. Green, G. W. Morley, M. E. Newton, J. G. Rarity, M. J. Booth, J. M. Smith, *Nat. Photonics* **2017**, *11*, 77.
[59] S. Castelletto, B. C. Johnson, A. Boretti, *IOP Conf. Ser.: Mater. Sci. Eng.* **2020**, *840*, 012010.
[60] L. Childress, R. Hanson, *MRS Bull.* **2013**, *38*, 134.
[61] G. Davies, M. F. Hamer, *Proc. R. Soc. Lond. A* **1976**, *348*, 285.
[62] A. Lenef, S. C. Rand, *Phys. Rev. B* **1996**, *53*, 13441.
[63] A. Gali, *Nanophotonics* **2019**, *8*, 1907.
[64] A. Gali, E. Janzén, P. Deák, G. Kresse, E. Kaxiras, *Phys. Rev. Lett.* **2009**, *103*, 186404.
[65] A. Alkauskas, B. B. Buckley, D. D. Awschalom, C. G. Van de Walle, *New J. Phys.* **2014**, *16*, 073026.
[66] V. Ivády, H. Zheng, A. Wickenbrock, L. Bougas, G. Chatzidrosos, K. Nakamura, H. Sumiya, T. Ohshima, J. Isoya, D. Budker, I. A. Abrikosov, A. Gali, *Phys. Rev. B* **2021**, *103*, 035307.
[67] J. M. Taylor, P. Cappellaro, L. Childress, L. Jiang, D. Budker, P. R. Hemmer, A. Yacoby, R. Walsworth, M. D. Lukin, *Nat. Phys.* **2008**, *4*, 810.
[68] J. R. Maze, P. L. Stanwix, J. S. Hodges, S. Hong, J. M. Taylor, P. Cappellaro, L. Jiang, M. V. G. Dutt, E. Togan, A. S. Zibrov, A. Yacoby, R. L. Walsworth, M. D. Lukin, *Nature* **2008**, *455*, 644.
[69] V. M. Acosta, E. Bauch, M. P. Ledbetter, A. Waxman, L.-S. Bouchard, D. Budker, *Phys. Rev. Lett.* **2010**, *104*, 070801.
[70] X.-D. Chen, C.-H. Dong, F.-W. Sun, C.-L. Zou, J.-M. Cui, Z.-F. Han, G.-C. Guo, *Appl. Phys. Lett.* **2011**, *99*, 161903.
[71] P. Neumann, I. Jakobi, F. Dolde, C. Burk, R. Reuter, G. Waldherr, J. Honert, T. Wolf, A. Brunner, J. H. Shim, D. Suter, H. Sumiya, J. Isoya, J. Wrachtrup, *Nano Lett.* **2013**, *13*, 2738.

[72] D. M. Toyli, C. F. de las Casas, D. J. Christle, V. V. Dobrovitski, D. D. Awschalom, *Proc. Natl. Acad. Sci. USA* **2013**, *110*, 8417.
[73] E. Neu, D. Steinmetz, J. Riedrich-Möller, S. Gsell, M. Fischer, M. Schreck, C. Becher, *New J. Phys.* **2011**, *13*, 025012.
[74] Y. Zhou, A. Rasmita, K. Li, Q. Xiong, I. Aharonovich, W.-b. Gao, *Nat. Commun.* **2017**, *8*, 14451.
[75] L. J. Rogers, K. D. Jahnke, M. H. Metsch, A. Sipahigil, J. M. Binder, T. Teraji, H. Sumiya, J. Isoya, M. D. Lukin, P. Hemmer, F. Jelezko, *Phys. Rev. Lett.* **2014**, *113*, 263602.
[76] D. D. Sukachev, A. Sipahigil, C. T. Nguyen, M. K. Bhaskar, R. E. Evans, F. Jelezko, M. D. Lukin, *Phys. Rev. Lett.* **2017**, *119*, 223602.
[77] K. D. Jahnke, A. Sipahigil, J. M. Binder, M. W. Doherty, M. Metsch, L. J. Rogers, N. B. Manson, M. D. Lukin, F. Jelezko, *New J. Phys.* **2015**, *17*, 043011.
[78] B. C. Rose, D. Huang, Z.-H. Zhang, P. Stevenson, A. M. Tyryshkin, S. Sangtawesin, S. Srinivasan, L. Loudin, M. L. Markham, A. M. Edmonds, D. J. Twitchen, S. A. Lyon, N. P. de Leon, *Science* **2018**, *361*, 60.
[79] Z.-H. Zhang, P. Stevenson, G. Thiering, B. C. Rose, D. Huang, A. M. Edmonds, M. L. Markham, S. A. Lyon, A. Gali, N. P. de Leon, *Phys. Rev. Lett.* **2020**, *125*, 237402.
[80] T. Iwasaki, F. Ishibashi, Y. Miyamoto, Y. Doi, S. Kobayashi, T. Miyazaki, K. Tahara, K. D. Jahnke, L. J. Rogers, B. Naydenov, F. Jelezko, S. Yamasaki, S. Nagamachi, T. Inubushi, N. Mizuochi, M. Hatano, *Sci. Rep.* **2015**, *5*, 12882.
[81] M. K. Bhaskar, D. D. Sukachev, A. Sipahigil, R. E. Evans, M. J. Burek, C. T. Nguyen, L. J. Rogers, P. Siyushev, M. H. M. abd H. Park, F. Jelezko, M. Loncar, M. D. Lukin, *Phys. Rev. Lett.* **2017**, *118*, 223603.
[82] G. Thiering, A. Gali, *Phys. Rev. X* **2018**, *8*, 021063.
[83] T. Iwasaki, Y. Miyamoto, T. Taniguchi, P. Siyushev, M. H. Metsch, F. Jelezko, M. Hatano, *Phys. Rev. Lett.* **2017**, *119*, 253601.
[84] A. L. Falk, B. B. Buckley, G. Calusine, W. F. Koehl, V. V. Dobrovitski, A. Politi, C. A. Zorman, P. X.-L. Feng, D. D. Awschalom, *Nat. Commun.* **2013**, *4*, 1819.
[85] L. Gordon, A. Janotti, C. G. Van de Walle, *Phys. Rev. B* **2015**, *92*, 045208.
[86] *Defects in Semiconductors* (Eds: N. Iwamoto, B. G. Svensson, In L. Romano, V. Privitera, C. Jagadish), Semiconductors and Semimetals, Vol. *91*, Elsevier, San Diego, CA **2015**, pp. 369–407.
[87] S. Castelletto, B. C. Johnson, V. Ivády, N. Stavrias, T. Umeda, A. Gali, T. Oshima, *Nat. Mater.* **2014**, *13*, 151.
[88] W. F. Koehl, B. B. Buckley, F. J. Heremans, G. Calusine, D. D. Awschalom, *Nature* **2011**, *479*, 84.
[89] Z. Mu, S. A. Zargaleh, H. J. von Bardeleben, J. E. Fröch, M. Nonahal, H. Cai, X. Yang, J. Yang, X. Li, I. Aharonovich, W. Gao, *Nano Lett.* **2020**, *20*, 6142.
[90] H. Singh, A. N. Anisimov, P. G. Baranov, D. Suter, *Phys. Rev. B* **2021**, *103*, 104103.
[91] T. Umeda, N. T. Son, J. Isoya, E. Janzén, T. Ohshima, N. Morishita, H. Itoh, A. Gali, M. Bockstedte, *Phys. Rev. Lett.* **2006**, *96*, 145501.
[92] E. Sörman, N. T. Son, W. M. Chen, O. Kordina, C. Hallin, E. Janzén, *Phys. Rev. B* **2000**, *61*, 2613.
[93] M. Wagner, B. Magnusson, W. M. Chen, E. Janzén, E. Sörman, C. Hallin, J. L. Lindström, *Phys. Rev. B* **2000**, *62*, 16555.
[94] E. Janzén, A. Gali, P. Carlsson, A. Gällström, B. Magnusson, N. Son, *Physica B* **2009**, *404*, 4354.
[95] A. Gali, *Mater. Sci. Forum* **2012**, *717–720*, 255.
[96] V. Ivády, J. Davidsson, N. T. Son, T. Ohshima, I. A. Abrikosov, A. Gali, *Phys. Rev. B* **2017**, *96*, 161114(R).
[97] P. Udvarhelyi, G. Thiering, N. Morioka, C. Babin, F. Kaiser, D. Lukin, T. Ohshima, J. Ul Hassan, N. T. Son, J. Vučković, J. Wrachtrup, A. Gali, *Phys. Rev. Appl.* **2020**, *13*, 054017.
[98] M. E. Bathen, L. Vines, J. Coutinho, *J. Phys.: Condens. Matter* **2020**, *33*, 075502.
[99] J. Davidsson, V. Ivády, R. Armiento, T. Ohshima, N. T. Son, A. Gali, I. A. Abrikosov, *Appl. Phys. Lett.* **2019**, *114*, 112107.
[100] R. Nagy, M. Niethammer, M. Widmann, Y.-C. Chen, P. Udvarhelyi, C. Bonato, J. Ul Hassan, R. Karhu, I. G. Ivanov, N. T. Son, J. R. Maze, T. Oshima, Ö. O. Soykal, A. Galí, S.-Y. Lee, F. Kaiser, J. Wrachtrup, *Nat. Commun.* **2019**, *10*, 1054.
[101] H. Singh, A. N. Anisimov, S. S. Nagalyuk, E. N. Mokhov, P. G. Baranov, D. Suter, *Phys. Rev. B* **2020**, *101*, 134110.
[102] H. Kraus, V. A. Soltamov, F. Fuchs, D. Simin, A. Sperlich, P. G. Baranov, G. V. Astakhov, V. Dyakonov, *Sci. Rep.* **2014**, *4*, 5303.
[103] A. N. Anisimov, D. Simin, V. A. Soltamov, S. P. Lebedev, P. G. Baranov, G. V. Astakhov, V. Dyakonov, *Sci. Rep.* **2016**, *6*, 33301.
[104] M. Niethammer, M. Widmann, S.-Y. Lee, P. Stenberg, O. Kordina, T. Ohshima, N. T. Son, E. Janzén, J. Wrachtrup, *Phys. Rev. Appl.* **2016**, *6*, 034001.
[105] D. Simin, V. A. Soltamov, A. V. Poshakinskiy, A. N. Anisimov, R. A. Babunts, D. O. Tolmachev, E. N. Mokhov, M. Trupke, S. A. Tarasenko, A. Sperlich, P. G. Baranov, V. Dyakonov, G. V. Astakhov, *Phys. Rev. X* **2016**, *6*, 031014.
[106] Ö. O. Soykal, P. Dev, S. E. Economou, *Phys. Rev. B* **2016**, *93*, 081207(R).
[107] S. E. Economou, P. Dev, *Nanotechnology* **2016**, *27*, 504001.
[108] V. A. Soltamov, C. Kasper, A. V. Poshakinskiy, A. N. Anisimov, E. N. Mokhov, A. Sperlich, S. A. Tarasenko, P. G. Baranov, G. V. Astakhov, V. Dyakonov, *Nat. Commun.* **2019**, *10*, 1678.
[109] J. W. Steeds, *Phys. Rev. B* **2009**, *80*, 245202.
[110] R. M. Karsthof, M. E. Bathen, A. Galeckas, L. Vines, *Phys. Rev. B* **2020**, *102*, 184111.
[111] D. J. Christle, A. L. Falk, P. Andrich, P. V. Klimov, J. Ul Hassan, N. T. Son, E. Janzén, T. Oshima, D. D. Awschalom, *Nat. Mater.* **2015**, *14*, 160.
[112] J. Davidsson, V. Ivády, R. Armiento, N. T. Son, A. Gali, I. A. Abrikosov, *New J. Phys.* **2018**, *20*, 023035.
[113] M. Bockstedte, F. Schütz, T. Garratt, V. Ivády, A. Gali, *npj Quantum Mater.* **2018**, *3*, 31.
[114] V. Ivády, I. A. Abrikosov, A. Gali, *npj Comput. Mater.* **2018**, *4*, 76.
[115] V. Ivády, *Phys. Rev. B* **2020**, *101*, 155203.
[116] H. Seo, A. L. Falk, P. V. Klimov, K. C. Miao, G. Galli, D. D. Awschalom, *Nat. Commun.* **2016**, *7*, 12935.
[117] K. C. Miao, J. P. Blanton, C. P. Anderson, A. Bourassa, A. L. Crook, G. Wolfowicz, H. Abe, T. Ohshima, D. D. Awschalom, *Science* **2020**, *369*, 1493.
[118] P. V. Klimov, A. L. Falk, D. J. Christle, V. V. Dobrovitski, D. D. Awschalom, *Sci. Adv.* **2015**, *1*, e1501015.
[119] A. Bourassa, C. P. Anderson, K. C. Miao, M. Onizhuk, H. Ma, A. L. Crook, H. Abe, J. Ul Hassan, T. Ohshima, N. T. Son, G. Galli, D. D. Awschalom, *Nat. Mater.* **2020**.
[120] S. A. Zargaleh, B. Eble, S. Hameau, J.-L. Cantin, L. Legrand, M. Bernard, F. Margaillan, J.-S. Lauret, J.-F. Roch, H. J. von Bardeleben, E. Rauls, U. Gerstmann, F. Treussart, *Phys. Rev. B* **2016**, *94*, 060102(R).
[121] S. A. Zargaleh, S. Hameau, B. Eble, F. Margaillan, H. J. von Bardeleben, J. L. Cantin, W. Gao, *Phys. Rev. B* **2018**, *98*, 165203.
[122] L. Spindlberger, A. Csóré, G. Thiering, S. Putz, R. Karhu, J. Ul Hassan, N. T. Son, T. Fromherz, A. Gali, M. Trupke, *Phys. Rev. Appl.* **2019**, *12*, 014015.
[123] A. Csóré, A. Gali, *Phys. Rev. B* **2020**, *102*, 241201(R).
[124] N. T. Son, A. Ellison, B. Magnusson, M. F. MacMillan, W. M. Chen, B. Monemar, E. Janzén, *J. Appl. Phys.* **1999**, *86*, 4348.
[125] W. F. Koehl, B. Diler, S. J. Whiteley, A. Bourassa, N. T. Son, E. Janzén, D. D. Awschalom, *Phys. Rev. B* **2017**, *95*, 035207.

[126] T. Bosma, G. J. J. Lof, C. M. Gilardoni, O. V. Zwier, F. Hendriks, B. Magnusson, A. Ellison, A. Gällström, I. G. Ivanov, N. T. Son, R. W. A. Havenith, C. H. van der Wal, *npj Quantum Inf.* **2018**, *4*, 48.
[127] N. T. Son, X. T. Trinh, A. Gällström, S. Leone, O. Kordina, E. Janzén, K. Szász, V. Ivády, A. Gali, *J. Appl. Phys.* **2012**, *112*, 083711.
[128] A. Gällström, B. Magnusson, F. C. Beyer, A. Gali, N. T. Son, S. Leone, I. G. Ivanov, C. G. Hemmingsson, A. Henry, E. Janzén, *Physica B* **2012**, *407*, 1462.
[129] K. M. Lee, L. S. Dang, G. D. Watkins, W. J. Choyke, *Phys. Rev. B* **1985**, *32*, 2273.
[130] A. Durand, Y. Baron, W. Redjem, T. Herzig, A. Benali, S. Pezzagna, J. Meijer, A. Y. Kuznetsov, J.-M. Gérard, I. Robert-Philip, M. Abbarchi, V. Jacques, G. Cassabois, A. Dréau, *Phys. Rev. Lett.* **2021**, *126*, 083602.
[131] W. Redjem, A. Durand, T. Herzig, A. Benali, S. Pezzagna, J. Meijer, A. Y. Kuznetsov, H. S. Nguyen, S. Cueff, J.-M. Gérard, I. Robert-Philip, B. Gil, D. Caliste, P. Pochet, M. Abbarchi, V. Jacques, A. Dréau, G. Cassabois, *Nat. Electron.* **2020**, *3*, 738.
[132] M. Toth, I. Aharonovich, *Annu. Rev. Phys. Chem.* **2019**, *70*, 123.
[133] T. T. Tran, C. Elbadawi, D. Totonjian, C. J. Lobo, G. Grosso, H. Moon, D. R. Englund, M. J. Ford, I. Aharonovich, M. Toth, *ACS Nano* **2016**, *10*, 7331.
[134] T. T. Tran, K. Bray, M. J. Ford, M. Toth, I. Aharonovich, *Nat. Nanotechnol.* **2016**, *11*, 37.
[135] F. Hayee, L. Yu, J. L. Zhang, C. J. Ciccarino, M. Nguyen, A. F. Marshall, I. Aharonovich, J. Vučković, P. Narang, T. F. Heinz, J. A. Dionne, *Nat. Mater.* **2020**, *19*, 534.
[136] L. Weston, D. Wickramaratne, M. Mackoit, A. Alkauskas, C. G. Van de Walle, *Phys. Rev. B* **2018**, *97*, 214104.
[137] M. Abdi, J.-P. Chou, A. Gali, M. B. Plenio, *ACS Photonics* **2018**, *5*, 1967.
[138] V. Ivády, G. Barcza, G. Thiering, S. Li, H. Hamdi, J.-P. Chou, Ö. Legeza, A. Gali, *npj Comput. Mater.* **2020**, *6*, 41.
[139] M. E. Turiansky, A. Alkauskas, C. G. Van de Walle, *Nat. Mater.* **2020**, *19*, 487.
[140] A. Sajid, M. J. Ford, J. R. Reimers, *Rep. Prog. Phys.* **2020**, *82*, 044501.
[141] C. Chakraborty, L. Kinnischtzke, K. M. Goodfellow, R. Beams, A. N. Vamivakas, *Nat. Nanotechnol.* **2015**, *10*, 507.
[142] P. Tonndorf, R. Schmidt, R. Schneider, J. Kern, M. Buschema, G. A. Steele, A. Castellanos-Gomez, H. S. J. van der Zant, S. M. de Vasconcellos, R. Bratschitsch, *Optica* **2015**, *2*, 347.
[143] A. Branny, S. Kumar, R. Proux, B. D. Gerardot, *Nat. Commun.* **2017**, *8*, 15053.
[144] A. M. Berhane, K.-Y. Jeong, C. Bradac, M. Walsh, D. Englund, M. Toth, I. Aharonovich, *Phys. Rev. B* **2018**, *97*, 165202.
[145] Y. Zhou, Z. Wang, A. Rasmita, S. Kim, A. Berhane, Z. Bodrog, G. Adamo, A. Gali, I. Aharonovich, W. bo Gao, *Sci. Adv.* **2018**, *4*, eaar3580.
[146] Y. Xue, H. Wang, N. Xie, Q. Yang, F. Xu, B. Shen, J. jie Shi, D. Jiang, X. Dou, T. Yu, B. quan Sun, *J. Phys. Chem. Lett.* **2020**, *11*, 2689.
[147] J. B. Varley, A. Janotti, C. G. Van de Walle, *Phys. Rev. B* **2016**, *93*, 161201(R).
[148] H. Seo, H. Ma, M. Govoni, G. Galli, *Phys. Rev. Mater.* **2017**, *1*, 075002.
[149] H. Baek, M. Brotons-Gisbert, Z. X. Koong, A. Campbell, M. Rambach, K. Watanabe, T. Taniguchi, B. D. Gerardot, *Sci. Adv.* **2020**, *6*, eaba8526.
[150] M. Ikezawa, Y. Sakuma, L. Zhang, Y. Sone, T. Mori, T. Hamano, M. Watanabe, K. Sakoda, Y. Masumoto, *Appl. Phys. Lett.* **2012**, *100*, 042106.
[151] N. Aslam, G. Waldherr, P. Neumann, F. Jelezko, J. Wrachtrup, *New J. Phys.* **2013**, *15*, 013064.
[152] P. Siyushev, H. Pinto, M. Vörös, A. Gali, F. Jelezko, J. Wrachtrup, *Phys. Rev. Lett.* **2013**, *110*, 167402.
[153] T. Lühmann, J. Küpper, S. Dietel, R. Staacke, J. Meijer, S. Pezzagna, *ACS Photonics* **2020**, *7*, 3376.
[154] G. Wolfowicz, C. P. Anderson, A. L. Yeats, S. J. Whiteley, J. Niklas, O. G. Poluektov, F. J. Heremans, D. D. Awschalom, *Nat. Commun.* **2017**, *8*, 1876.
[155] B. Magnusson, N. T. Son, A. Csóré, A. Gällström, T. Ohshima, A. Gali, I. G. Ivanov, *Phys. Rev. B* **2018**, *98*, 195202.
[156] G. Wolfowicz, S. J. Whiteley, D. D. Awschalom, *Proc. Natl. Acad. Sci. USA* **2018**, *115*, 7879.
[157] G. Wolfowicz, C. P. Anderson, S. J. Whiteley, D. D. Awschalom, *Appl. Phys. Lett.* **2019**, *115*, 043105.
[158] M. Rühl, L. Bergmann, M. Krieger, H. B. Weber, *Nano Lett.* **2020**, *20*, 658.
[159] C. F. de la Casas, D. J. Christle, J. Ul Hassan, T. Ohshima, N. T. Son, D. D. Awschalom, *Appl. Phys. Lett.* **2017**, *111*, 262403.
[160] M. Widmann, M. Niethammer, D. Y. Fedyanin, I. A. Khramtsov, T. Rendler, I. D. Booker, J. Ul Hassan, N. Morioka, Y.-C. Chen, I. G. Ivanov, N. T. Son, T. Ohshima, M. Bockstedte, A. Gali, C. Bonato, S.-Y. Lee, J. Wrachtrup, *Nano Lett.* **2019**, *19*, 7173.
[161] K. Bray, D. Y. Fedyanin, I. A. Khramtsov, M. O. Bilokur, B. Regan, M. Toth, I. Aharonovich, *Appl. Phys. Lett.* **2020**, *116*, 101103.
[162] N. T. Son, P. Stenberg, V. Jokubavicius, H. Abe, T. Ohshima, J. Ul Hassan, I. G. Ivanov, *Appl. Phys. Lett.* **2019**, *114*, 212105.
[163] M. L. David, G. Alfieri, E. M. Monakhov, A. Hallén, C. Blanchard, B. G. Svensson, J. F. Barbot, *J. Appl. Phys.* **2004**, *95*, 4728.
[164] E. Van Oort, M. Glasbeek, *Chem. Phys. Lett.* **1990**, *168*, 529.
[165] F. Dolde, H. Fedder, M. W. Doherty, T. Nöbauer, F. Rempp, G. Balasubramanian, T. Wolf, F. Reinhard, L. C. L. Hollenberg, F. Jelezko, J. Wrachtrup, *Nat. Phys.* **2011**, *7*, 459.
[166] M. Kim, H. J. Mamin, M. H. Sherwood, K. Ohno, D. D. Awschalom, D. Rugar, *Phys. Rev. Lett.* **2015**, *115*, 087602.
[167] S. Asaad, V. Mourik, B. Joecker, M. A. I. Johnson, A. D. Baczewski, H. R. Firgau, M. T. Madzik, V. Schmitt, J. J. Pla, F. E. Hudson, K. M. Itoh, J. C. McCallum, A. S. Dzurak, A. Laucht, A. Morello, *Nature* **2020**, *579*, 205.
[168] P. V. Klimov, A. L. Falk, B. B. Buckley, D. D. Awschalom, *Phys. Rev. Lett.* **2014**, *112*, 087601.
[169] M. Niethammer, M. Widmann, T. Rendler, N. Morioka, Y.-C. Chen, R. Stöhr, J. Ul Hassan, S. Onoda, T. Ohshima, S.-Y. Lee, A. Mukherjee, J. Isoya, N. T. Son, J. Wrachtrup, *Nat. Commun.* **2019**, *10*, 5569.
[170] A. Lohrmann, N. Iwamoto, Z. Bodrog, S. Castelletto, T. Ohshima, T. J. Karle, A. Gali, S. Prawer, J. C. McCallum, B. C. Johnson, *Nat. Commun.* **2015**, *6*, 7783.
[171] H. F. Fotso, A. E. Feiguin, D. D. Awschalom, V. V. Dobrovitski, *Phys. Rev. Lett.* **2016**, *116*, 033603.
[172] D. M. Lukin, A. D. White, R. Trivedi, M. A. Guidry, N. Morioka, C. Babin, Ö. O. Soykal, J. Ul-Hassan, N. T. Son, T. Ohshima, P. K. Vasireddy, M. H. Nasr, S. Sun, J.-P. W. MacLean, C. Dory, E. A. Nanni, J. Wrachtrup, F. Kaiser, J. Vučković, *npj Quantum Inf.* **2020**, *6*, 80.
[173] J. Stark, *Ann. Phys.* **1914**, *50*, 489.
[174] A. M. Stoneham, *Theory of Defects in Solids: Electronic Structure of Defects in Insulators and Semiconductors*, Clarendon Press, Oxford, UK **2001**.
[175] P. Tamarat, T. Gaebel, J. R. Rabeau, M. Khan, A. D. Greentree, H. Wilson, L. C. L. Hollenberg, S. Prawer, P. Hemmer, F. Jelezko, J. Wrachtrup, *Phys. Rev. Lett.* **2006**, *97*, 083002.
[176] L. C. Bassett, F. J. Heremans, C. G. Yale, B. B. Buckley, D. D. Awschalom, *Phys. Rev. Lett.* **2011**, *107*, 266403.
[177] T. Müller, I. Aharonovich, L. Lombez, Y. Alaverdyan, A. N. Vamivakas, S. Castelletto, F. Jelezko, J. Wrachtrup, S. Prawer, M. Atatüre, *New J. Phys.* **2011**, *13*, 075001.
[178] K. C. Miao, A. Bourassa, C. P. Anderson, S. J. Whiteley, A. L. Crook, S. L. Bayliss, G. Wolfowicz, G. Thiering, P. Udvarhelyi, V. Ivády, H. Abe, T. Ohshima, Á. Gali, D. D. Awschalom, *Sci. Adv.* **2019**, *5*, eaay0527.

[179] S. A. Empedocles, M. G. Bawendi, *Science* **1997**, *278*, 2114.
[180] C. Brunel, P. Tamarat, B. Lounis, J. C. Woehl, M. Orrit, *J. Phys. Chem. A* **1999**, *103*, 2429.
[181] B. F. Garrett, I. Azuri, L. Kronik, J. R. Chelikowsky, *J. Chem. Phys.* **2016**, *145*, 174111.
[182] G. Noh, D. Choi, J.-H. Kim, D.-G. Im, Y.-H. Kim, H. Seo, J. Lee, *Nano Lett.* **2018**, *18*, 4710.
[183] K. Kunc, R. Resta, *Phys. Rev. Lett.* **1983**, *51*, 686.
[184] P. Udvarhelyi, R. Nagy, F. Kaiser, S.-Y. Lee, J. Wrachtrup, A. Gali, *Phys. Rev. Appl.* **2019**, *11*, 044022.
[185] N. Nikolay, N. Mendelson, N. Sadzak, F. Böhm, T. T. Tran, B. Sontheimer, I. Aharonovich, O. Benson, *Phys. Rev. Appl.* **2019**, *11*, 041001.
[186] A. Scavuzzo, S. Mangel, J.-H. Park, S. Lee, D. L. Duong, C. Strelow, A. Mews, M. Burghard, K. Kern, *Appl. Phys. Lett.* **2019**, *114*, 062104.
[187] Y. Xia, Q. Li, J. Kim, W. Bao, C. Gong, S. Yang, Y. Wang, X. Zhang, *Nano Lett.* **2019**, *19*, 7100.
[188] C. Chakraborty, N. R. Jungwirth, G. D. Fuchs, A. N. Vamivakas, *Phys. Rev. B* **2019**, *99*, 045308.
[189] K. G. Schädler, C. Ciancico, S. Pazzagli, P. Lombardi, A. Bachtold, C. Toninelli, A. Reserbat-Plantey, F. H. L. Koppens, *Nano Lett.* **2019**, *6*, 3789.
[190] P. Olivero, F. Bosia, B. A. Fairchild, B. C. Gibson, A. D. Greentree, P. Spizzirri, S. Prawer, *New J. Phys.* **2013**, *15*, 043027.
[191] S. Hsieh, P. Bhattacharyya, C. Zu, T. Mittiga, T. J. Smart, F. Machado, B. Kobrin, T. O. Höhn, N. Z. Rui, M. Kamrani, S. Chatterjee, S. Choi, M. Zaletel, V. V. Struzhkin, J. E. Moore, V. I. Levitas, R. Jeanloz, N. Y. Yao, *Science* **2019**, *366*, 1349.
[192] A. Barfuss, J. Teissier, E. Neu, A. Nunnenkamp, P. Maletinsky, *Nat. Phys.* **2015**, *11*, 820.
[193] P. Ovartchaiyapong, K. W. Lee, B. A. Myers, A. C. B. Jayich, *Nat. Commun.* **2014**, *5*, 4429.
[194] D. A. Broadway, B. C. Johnson, M. S. J. Barson, S. E. Lillie, N. Dontschuk, D. J. McCloskey, A. Tsai, T. Teraji, D. A. Simpson, A. Stacey, J. C. McCallum, J. E. Bradby, M. W. Doherty, L. C. L. Hollenberg, J.-P. Tetienne, *Nano Lett.* **2019**, *19*, 4543.
[195] Z. Xu, Z. qi Yin, Q. Han, T. Li, *Opt. Mater. Express* **2019**, *9*, 4654.
[196] S. Meesala, Y.-I. Sohn, B. Pingault, L. Shao, H. A. Atikian, J. Holzgrafe, M. Gündogan, C. Stavrakas, A. Sipahigil, C. Chia, R. Evans, M. J. Burek, M. Zhang, L. Wu, J. L. Pacheco, J. Abraham, E. Bielejec, M. D. Lukin, M. Atatüre, M. Loncar, *Phys. Rev. B* **2018**, *97*, 205444.
[197] B. Machielse, S. Bogdanovic, S. Meesala, S. Gauthier, M. J. Burek, G. Joe, M. Chalupnik, Y. I. Sohn, J. Holzgrafe, R. E. Evans, C. Chia, H. Atikian, M. K. Bhaskar, D. D. Sukachev, L. Shao, S. Maity, M. D. Lukin, M. Loncar, *Phys. Rev. X* **2019**, *9*, 031022.
[198] P. Udvarhelyi, V. O. Shkolnikov, A. Gali, G. Burkard, A. Pályi, *Phys. Rev. B* **2018**, *98*, 075201.
[199] P. Udvarhelyi, A. Gali, *Phys. Rev. Appl.* **2018**, *10*, 054010.
[200] A. L. Falk, P. V. Klimov, B. B. Buckley, V. Ivády, I. A. Abrikosov, G. Calusine, W. F. Koehl, A. Gali, D. D. Awschalom, *Phys. Rev. Lett.* **2014**, *112*, 187601.
[201] G. C. Vásquez, M. E. Bathen, A. Galeckas, C. Bazioti, K. M. Johansen, D. Maestre, A. Cremades, . Prytz, A. M. Moe, A. Y. Kuznetsov, L. Vines, *Nano Lett.* **2020**, *20*, 8689.
[202] N. Mendelson, M. Doherty, M. Toth, I. Aharonovich, T. T. Tran, *Adv. Mater.* **2020**, *32*, 1908316.
[203] S. Li, J.-P. Chou, A. Hu, M. B. Plenio, P. Udvarhelyi, G. Thiering, M. Abdi, A. Gali, *npj Quantum Inf.* **2020**, *6*, 85.
[204] O. Iff, D. Tedeschi, J. Martín-Sánchez, M. Moczala-Dusanowska, S. Tongay, K. Yumigeta, J. Taboada-Gutiérres, M. Savaresi, A. Rastelli, P. Alonso-González, S. Höfling, R. Trotta, C. Schneider, *Nano Lett.* **2019**, *19*, 6931.
[205] A. Alkauskas, M. D. McCluskey, C. G. Van de Walle, *J. Appl. Phys.* **2016**, *119*, 181101.
[206] A. Alkauskas, J. L. Lyons, D. Steiauf, C. G. Van de Walle, *Phys. Rev. Lett.* **2012**, *109*, 267401.
[207] A. Hashemi, C. Linderalv, A. V. Krasheninnikov, T. Ala-Nissila, P. Erhart, H.-P. Komsa, unpublished **2020**.
[208] Z. Shang, A. Hashemi, Y. Berencén, H.-P. Komsa, P. Erhart, S. Zhou, M. Helm, A. V. Krasheninnikov, G. V. Astakhov, *Phys. Rev. B* **2020**, *101*, 144109.
[209] K. J. Satzinger, Y. P. Zhong, H.-S. Chang, G. A. Peairs, A. Bienfait, M.-H. Chou, A. Y. Cleland, C. R. Conner, É. Dumur, J. Grebel, I. Gutierrez, B. H. November, R. G. Povey, S. J. Whiteley, D. D. Awschalom, D. I. Schuster, A. N. Cleland, *Nature* **2018**, *563*, 661.
[210] S. Hong, M. S. Grinolds, P. Maletinsky, R. L. Walsworth, M. D. Lukin, A. Yacoby, *Nano Lett.* **2012**, *12*, 3920.
[211] S. J. Whiteley, G. Wolfowicz, C. P. Anderson, A. Bourassa, H. Ma, M. Ye, G. Koolstra, K. J. Satzinger, M. V. Holt, F. J. Heremans, A. N. Cleland, D. I. Schuster, G. Galli, D. D. Awschalom, *Nat. Phys.* **2019**, *15*, 490.
[212] A. Berhane, S. Choi, H. Kato, T. Makino, N. Mizuochi, S. Yamasaki, I. Aharonovich, *Appl. Phys. Lett.* **2015**, *106*, 171102.
[213] D. Y. Fedyanin, M. Agio, *New J. Phys.* **2016**, *18*, 073012.
[214] F. M. Hrubesch, G. Braunbeck, M. Stutzmann, F. Reinhard, M. S. Brandt, *Phys. Rev. Lett.* **2017**, *118*, 037601.
[215] P. Siyushev, M. Nesladek, E. Bourgeois, M. Gulka, J. Hruby, T. Yamamoto, M. Trupke, T. Teraji, J. Isoya, F. Jelezko, *Science* **2019**, *363*, 728.
[216] M. Widmann, M. Niethammer, T. Makino, T. Rendler, S. Lasse, T. Ohshima, J. Ul Hassan, N. T. Son, S.-Y. Lee, J. Wrachtrup, *Appl. Phys. Lett.* **2018**, *112*, 231103.
[217] F. Sardi, T. Kornher, M. Widmann, R. Kolesov, F. Schiller, T. Reindl, M. Hagel, J. Wrachtrup, *Appl. Phys. Lett.* **2020**, *117*, 022105.
[218] F. Garrisi, I. Chatzopoulos, R. Cernansky, A. Politi, unpublished **2020**.
[219] M. Radulaski, M. Widmann, M. Niethammer, J. L. Zhang, S.-Y. Lee, T. Rendler, K. G. Lagoudakis, N. T. Son, E. Janzén, T. Oshima, J. Wrachtrup, J. Vucković, *Nano Lett.* **2017**, *17*, 1782.
[220] B. Zhang, S. He, Q. Yang, H. Lu, L. Wang, F. Chen, *Appl. Phys. Lett.* **2020**, *116*, 111903.
[221] S. Castelletto, B. C. Johnson, C. Zachreson, D. Beke, I. Balogh, T. Ohshima, I. Aharonovich, A. Gali, *ACS Nano* **2014**, *8*, 7938.
[222] N. H. Wan, T.-J. Lu, K. C. Chen, M. P. Walsh, M. E. Trusheim, L. De Santis, E. A. Bersin, I. B. Harris, S. L. Mouradian, I. R. Christen, E. S. Bielejec, D. Englund, *Nature* **2020**, *583*, 226.
[223] J. L. Zhang, S. Sun, M. J. Burek, C. Dory, Y.-K. Tzeng, K. A. Fischer, Y. Kelaita, K. G. Lagoudakis, M. Radulaski, Z.-X. Shen, N. A. Melosh, S. Chu, M. Loncar, J. Vucković, *Nano Lett.* **2018**, *18*, 1360.
[224] A. Faraon, P. E. Barclay, C. Santori, K.-M. C. Fu, R. G. Beausoleil, *Nat. Photonics* **2011**, *5*, 301.
[225] A. Faraon, C. Santori, Z. Huang, V. M. Acosta, R. G. Beausoleil, *Phys. Rev. Lett.* **2012**, *109*, 033604.
[226] T. Schröder, F. Gädeke, M. J. Banholzer, O. Benson, *New J. Phys.* **2011**, *13*, 055017.
[227] D. Simin, H. Kraus, A. Sperlich, T. Ohshima, G. V. Astakhov, V. Dyakonov, *Phys. Rev. B* **2017**, *95*, 161201(R).
[228] L. J. Martínez, T. Pelini, V. Waselowski, J. R. Maze, B. Gil, G. Cassabois, V. Jacques, *Phys. Rev. B* **2016**, *94*, 121405(R).
[229] G. Grosso, H. Moon, B. Lienhard, S. Ali, D. K. Efetov, M. M. Furchi, P. Jarillo-Herrero, M. J. Ford, I. Aharonovich, D. Englund, *Nat. Commun.* **2017**, *8*, 705.
[230] C. Chakraborty, K. M. Goodfellow, S. Dhara, A. Yoshimura, V. Meunier, A. N. Vamivakas, *Nano Lett.* **2017**, *17*, 2253.
[231] L. Sapienza, M. Davanco, A. Badolato, K. Srinivasan, *Nat. Commun.* **2015**, *6*, 7833.

[232] M. A. Guidry, K. Y. Yang, D. M. Lukin, A. Markosyan, J. Yang, M. M. Fejer, J. Vučković, *Optica* **2020**, *7*, 1139.
[233] D. O. Bracher, X. Zhang, E. L. Hu, *Proc. Natl. Acad. Sci. USA* **2017**, *114*, 4060.
[234] M. N. Gadalla, A. S. Greenspon, R. Kuate Defo, X. Zhang, E. L. Hu, *Proc. Natl. Acad. Sci. USA* **2021**, *118*, e2021768118.
[235] D. M. Lukin, C. Dory, M. A. Guidry, K. Y. Yang, S. D. Mishra, R. Trivedi, M. Radulaski, S. Sun, D. Vercruysse, G. H. Ahn, J. Vučković, *Nat. Photonics* **2020**, *14*, 330.
[236] A. L. Crook, C. P. Anderson, K. C. Miao, A. Bourassa, H. Lee, S. L. Bayliss, D. O. Bracher, X. Zhang, H. Abe, T. Ohshima, E. L. Hu, D. D. Awschalom, *Nano Lett.* **2020**, *20*, 3427.
[237] B. J. M. Hausmann, I. Bulu, V. Venkataraman, P. Deotare, M. Loncar, *Nat. Photonics* **2014**, *8*, 369.
[238] M. J. Burek, Y. Chu, M. S. Z. Liddy, P. Patel, J. Rochman, S. Meesala, W. Hong, Q. Quan, M. D. Lukin, M. Loncar, *Nat. Commun.* **2014**, *5*, 5718.
[239] B.-S. Song, T. Asano, S. Jeon, H. Kim, C. Xen, D. D. Kang, S. Noda, *Optica* **2019**, *6*, 991.
[240] R. Wang, M. Ikezawa, Y. Sakuma, H. Takeda, N. Ikeda, Y. Sugimoto, K. Sakoda, Y. Yamada, Y. Masumoto, *ACS Photonics* **2020**, *7*, 321.
[241] A. W. Schell, H. Takashima, T. T. Tran, I. Aharonovich, *ACS Photonics* **2017**, *4*, 761.
[242] J. E. Fröch, S. Kim, N. Mendelson, M. Kianinia, M. Toth, I. Aharonovich, *ACS Nano* **2020**, *14*, 7085.
[243] L. C. Flatten, L. Weng, A. Branny, S. Johnson, P. R. Dolan, A. A. P. Trichet, B. D. Gerardot, J. M. Smith, *Appl. Phys. Lett.* **2018**, *112*, 191195.

Marianne Etzelmüller Bathen received her M.Sc. degree in nanotechnology from the Norwegian University of Science and Technology (NTNU) in 2016, and was awarded a Ph.D. in physics from the University of Oslo (UiO) in 2020. She is currently a postdoctoral researcher at ETH Zürich, where she combines density functional theory calculations with electro-optical measurements and semiconductor device fabrication to exploit semiconductor point defects for quantum technologies.

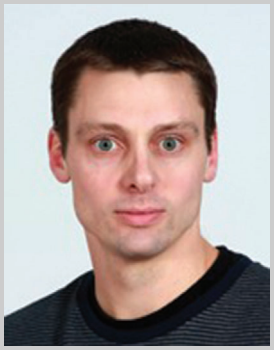

Lasse Vines was awarded an M.Sc. degree in physics and mathematics from the Norwegian University of Science and Technology (NTNU) in 2001. After a short time in industry, he completed a Ph.D. in physics at the University of Oslo in 2008. Since 2013, he is a professor in the Department of Physics at the University of Oslo, where he conducts and coordinates research on defects, doping and diffusion in semiconductors for applications within power electronics, solar cells and quantum technology.